

Supporting information

Carboxamide carbonyl-ruthenium(II) complexes: Detailed structural and mechanistic studies in the transfer hydrogenation of ketones

Robert T. Kumah†, Paranthaman, Vijayan †, and Stephen O. Ojwach†*

†*School of Chemistry and Physics, College of Agriculture, Engineering and Science,
University of KwaZulu-Natal, Private Bag X01, Scottsville, South Africa,

*Corresponding author: Tel.: +27 (33) 260 5239; Fax: +27 (33) 260 5009

E-mail: ojwach@ukzn.ac.za (S. O. Ojwach)

Table of contents

Entry	Item	Page
1	Synthesis of <i>N</i> -(benzo[d]thiazol-2-yl)pyrazine-2-carboxamide (HL1) and <i>N</i> -(1 <i>H</i> -benzo[d]imidazol-2-yl)pyrazine-2-carboxamide (HL2)	1
2	Table S1. Crystal data and structure refinement for complexes Ru1 , Ru2 and Ru4	3
3	Table S2. Selected bond lengths (Å) and bond angles (°) for Ru1 , Ru2 and Ru4	4
4	¹ H NMR spectra of ligands of HL1 and HL2 and complexes Ru1-Ru4 (Figures S1- S6)	5
5	³¹ C NMR spectra of carboxamide ligands HL1 and HL2 and complexes Ru1-Ru5 (Figures S7- S11)	8
6	³¹ P NMR spectra of complexes Ru1-Ru4 (Figures S12- S15)	11
7	FT-IR spectra of ligands, HL1 and HL2 and complexes Ru1-Ru4 (Figures S16- S21)	13
8	LR LC-MS spectral data of ligands, HL1 and HL2 and complexes Ru1-Ru4 (Figures S22- S27)	17
9	¹ H NMR spectra of TH of ketones reactions sampled at various reaction times (Figure S28- S44)	21
9	Kinetic graphs of the transfer hydrogenation reactions (Figures S45-S47)	34

4.3 Synthesis of the carboxamide ligands

4.3.1 *N*-(benzo[*d*]thiazol-2-yl)pyrazine-2-carboxamide (**HL1**)

Pyrazine-2-dicarboxylic acid (1.00 g, 5.02 mmol) and 2-aminobenzothiazole (0.75 g, 5.02 mmol) were dissolved in 20 mL pyridine and then heated with stirring for 15 minutes at 110 °C. Triphenylphosphite P(OPh)₃ (1.55 g, 5.00 mmol) was introduced drop-wise to the resulting solution and then allowed to stir at 90 °C for 12 h. The crude product was poured into ice-cold water, filtered, and washed with cold water and cold methanol. The yellow crude powder was recrystallized from methanol and toluene. Yield: 1.54 g (74%). ¹H NMR (400 MHz, *d*₆-DMSO): 9.37 (s, 1H_{amidate}), 8.98 (d, ³J_{HH} = 2.4 Hz, 1H_{pyz}), 8.90 – 8.85 (m, 1H_{pyz}), 8.07 (d, ³J_{HH} = 7.8 Hz, 1H_{pyz}), 7.84 (d, ³J_{HH} = 8.0 Hz, 1H_{bz}), 7.50 (t, ³J_{HH} = 7.6 Hz, 1H_{bz}), 7.38 (t, ³J_{HH} = 7.6 Hz, 1H_{bz}). ¹³C NMR (101 MHz, CDCl₃) δ: 161.3(C-carbonyl), 156.8(C-pyrazine), 148.6(C-pyrazine), 145.0(C-pyrazine), 143.1(C-pyrazine), 142.5(C-benzothiole), 132.5(C-benzothiole), 126.5(C-benzothiole), 124.4(C-benzothiole), 121.5(C-benzothiole), 121.4(C-benzothiole). FT-IR spectrum (Zn-Se ATR, cm⁻¹): 3324 (N–H), 1691 (C=O), 1533 (C=N). MS spectrum (m/z): Calcd. 510.04; Found 511.08 (2M⁺ - H). Anal. Cald. for: C₁₂H₈N₄OS: C, 56.24; H, 3.15; N, 21.86; S, 12.51%. Found: C, 56.11; H, 3.52; N, 21.64; S, 12.11%.

4.3.2 *N*-(1*H*-benzo[*d*]imidazol-2-yl)pyrazine-2-carboxamide (**HL2**)

Pyrazine-2-dicarboxylic acid (1.00 g, 5.00 mmol), 2-aminobenzothiazole (0.75 g, 5.00 mmol), and P(OPh)₃ (1.55 g, 5.00 mmol). Recrystallization was achieved from methanol to obtain a pale-yellow solid. Yield: 1.04 g (72%). ¹H NMR (400 MHz, DMSO) δ 12.20 (s, 1H_{amidate}), 9.37 (d, ³J_{HH} = 1.2 Hz, 1H_{pyz}), 8.86 (d, ³J_{HH} = 35.5, 1.9 Hz, 2H_{pyz}), 7.51 (d, ³J_{HH} = 5.9, 3.2 Hz, 2H_{bz}), 7.18 (dd, ³J_{HH} = 5.9, 3.2 Hz, 2H_{bz}). ¹³C NMR (101 MHz, CDCl₃) δ: 163.2(C_{carbonyl}), 149.9(C_{pyrazine}), 149.0(C_{pyrazine}), 138.6(C_{pyrazine}), 131.5(C_{pyrazine}),

127.6(C_{benzoimidazole}), 126.1(C_{benzoimidazole}), 126.5(C_{benzoimidazole}), 127.6(C_{benzoimidazole}),
126.1(C_{benzoimidazole}), 122.9(C_{benzoimidazole}). FT-IR spectrum ((Zn-Se ATR, cm⁻¹): 3251 (N-H),
1684 (C=O), 1546 (C=N). MS spectrum, m/z: calcd. 239.08; found 240.07 (M⁺ + H). Anal.
Cald. for: C₁₂H₉N₅O: C, 60.21; H, 3.79; N, 29.28; O, 6.69; Found: C, 60.11; H, 3.52; N, 29.64.

Table S1. Crystal data and structure refinement for complexes **Ru1**, **Ru2** and **Ru4**

	Ru1	Ru2	Ru4
Empirical formula	C ₉₉ H ₇₅ Cl ₄ N ₈ O ₄ P ₄ Ru ₂ S ₂	C ₅₀ H ₄₀ Cl ₂ N ₄ O ₂ P ₂ RuS	C ₄₉ H ₃₉ Cl ₂ N ₅ O ₂ P ₂ Ru
Formula weight	1972.61	994.83	963.76
Temperature	100(2) K	100(2) K	100(2) K
Wavelength	0.71073 Å	0.71073 Å	0.71073 Å
Crystal system	Monoclinic	Monoclinic	Monoclinic
Space group	P 21/c	P 21/n	P 21/n
Unit cell dimensions	a = 21.3269(17) Å b = 12.2526(10) Å c = 37.414(3) Å α = 90° β = 101.929(2)° γ = 90°	a = 12.1017(6) Å b = 13.8083(7) Å c = 27.2988(14) Å α = 90° β = 101.929(2)° γ = 90°	a = 9.8144(6) Å b = 18.5959(12) Å c = 23.1600(15) Å α = 90° β = 94.309(3)° γ = 90°
Volume	9685.9(14) Å ³	4463.2(4) Å ³	4214.9(5) Å ³
Z	4	4	4
Density (calculated)	1.353 Mg/m ³	1.480 Mg/m ³	1.519 Mg/m ³
Absorption coefficient	0.585 mm ⁻¹	0.636 mm ⁻¹	0.623 mm ⁻¹
F(000)	4020	2032	1968
Crystal size (mm ³)	0.260×0.200×0.140	0.23×0.14×0.08	0.640×0.440×0.240
Theta range for data collection	1.099 to 28.300°	1.525 to 28.165°	1.406 to 28.291°
Index ranges	-28 ≤ h ≤ 28, -16 ≤ k ≤ 16, -49 ≤ l ≤ 49	-16 ≤ h ≤ 15, -18 ≤ k ≤ 16, -36 ≤ l ≤ 36	-13 ≤ h ≤ 13, -24 ≤ k ≤ 22, -30 ≤ l ≤ 30
Reflections collected	176176	78016	76052
Independent reflections	24094 [R(int) = 0.0515]	10946 [R(int) = 0.0335]	10451 [R(int) = 0.0332]
Completeness to theta	100.0 %	100.0 %	99.9 %
Data / restraints / parameters	23990 / 0 / 1108	10882 / 0 / 563	10403 / 0 / 554
Goodness-of-fit on F ²	1.061	1.602	1.047
Final R indices [I > 2σ(I)]	R1 = 0.0638, wR2 = 0.1935	R1 = 0.0269, wR2 = 0.0627	R1 = 0.0410, wR2 = 0.1157
R indices (all data)	R1 = 0.0779, wR2 = 0.2063	R1 = 0.0324, wR2 = 0.0691	R1 = 0.0445, wR2 = 0.1186

Largest diff. peak and hole	4.897 and -2.779 e.Å ⁻³	0.645 and -0.664 e.Å ⁻³	1.803 and -1.997 e.Å ⁻³
-----------------------------	------------------------------------	------------------------------------	------------------------------------

Table S2. Selected bond lengths (Å) and bond angles (°) for **Ru1**, **Ru2** and **Ru4**

Ru1		Ru2		Ru4	
Ru(1)-C(49)	1.984(7)	Ru(1)-C(13)	1.8519(18)	Ru(1)-C(13)	1.984(7)
Ru(1)-N(1)	2.113(3)	Ru(1)-N(1)	2.1180(14)	Ru(1)-N(1)	2.113(3)
Ru(1)-N(2)	2.115(3)	Ru(1)-N(2)	2.116(14)	Ru(1)-N(2)	2.115(3)
Ru(1)-P(1)	2.4000(11)	Ru(1)-P(1)	2.3636(4)	Ru(1)-P(1)	2.4000(11)
Ru(1)-Cl(1)	2.4258(10)	Ru(1)-H(1A)	1.55(2)	Ru(1)-H(1A)	1.9672(10)
Ru1		Ru2		Ru4	
C(49)-Ru(1)-N(1)	176.32(16)	C(13)-Ru(1)-N(1)	177.73(7)	C(13)-Ru(1)-N(1)	100.81(10)
N(1)-Ru(1)-N(2)	77.84(13)	N(1)-Ru(1)-N(2)	76.13(5)	N(1)-Ru(1)-N(3)	76.24(8)
C(49)-Ru(1)-P(2)	89.04(13)	C(13)-Ru(1)-P(2)	90.76(5)	C(13)-Ru(1)-P(2)	89.05(8)
N(1)-Ru(1)-P(2)	91.12(9)	N(1)-Ru(1)-P(2)	88.31(4)	N(1)-Ru(1)-P(2)	95.06(6)
P(2)-Ru(1)-P(1)	176.88(4)	P(2)-Ru(1)-P(1)	165.302(16)	P(2)-Ru(1)-P(1)	168.60(2)

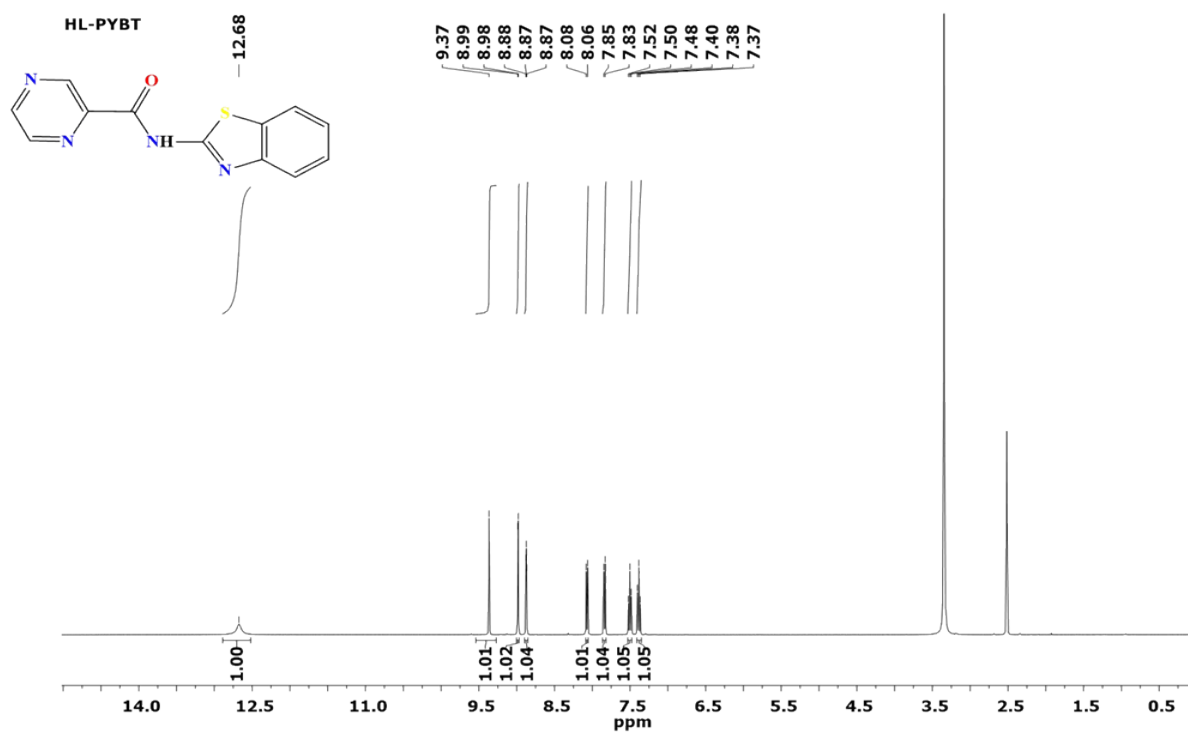


Figure S1. ^1H NMR spectrum (400 MHz, 298K d_6 -DMSO) of 1 *N*-(benzo[d]thiazol-2-yl)pyrazine-2-carboxamide ligand, **HL1** showing the diagnostic signal at δ_{H} :12.68 ppm and all key signals between δ_{H} : 7.37-9.37 ppm.

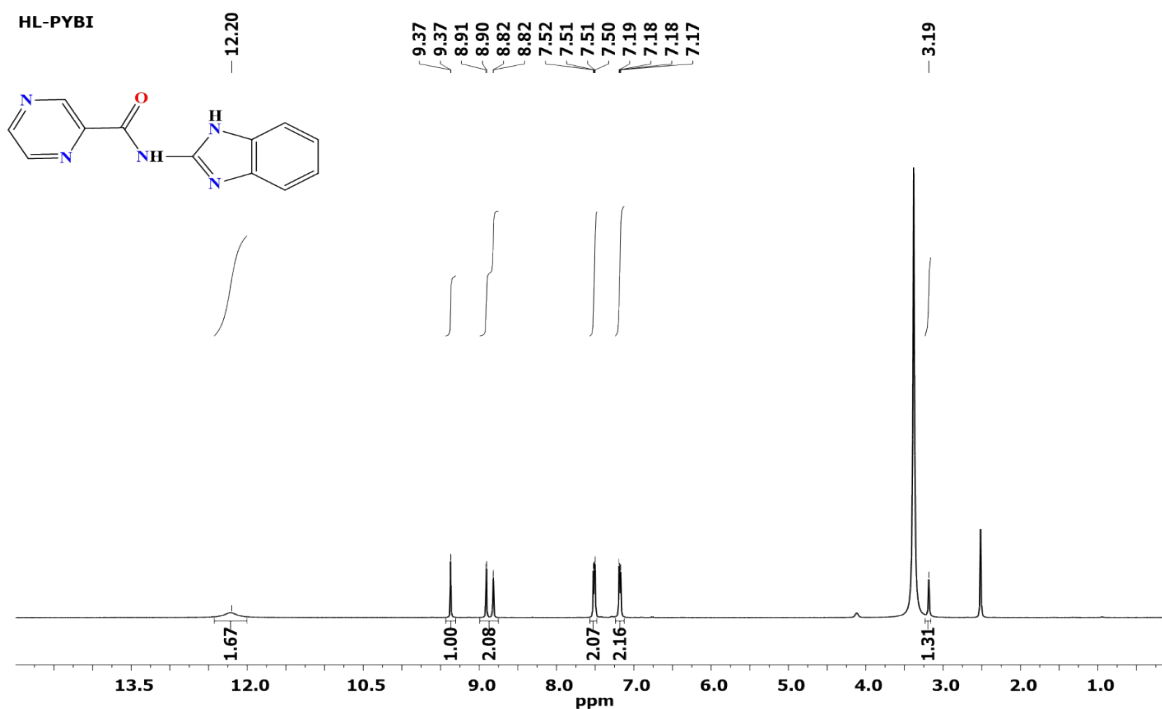


Figure S2. ^1H NMR spectrum (400 MHz, 298K d_6 -DMSO) of *N*-(1*H*-benzo[d]imidazol-2-yl)pyrazine-2-carboxamide ligand, **HL2** showing the signature peak at δ_{H} : 12.20 ppm and all key peaks between δ_{H} : 7.17-9.37 ppm.

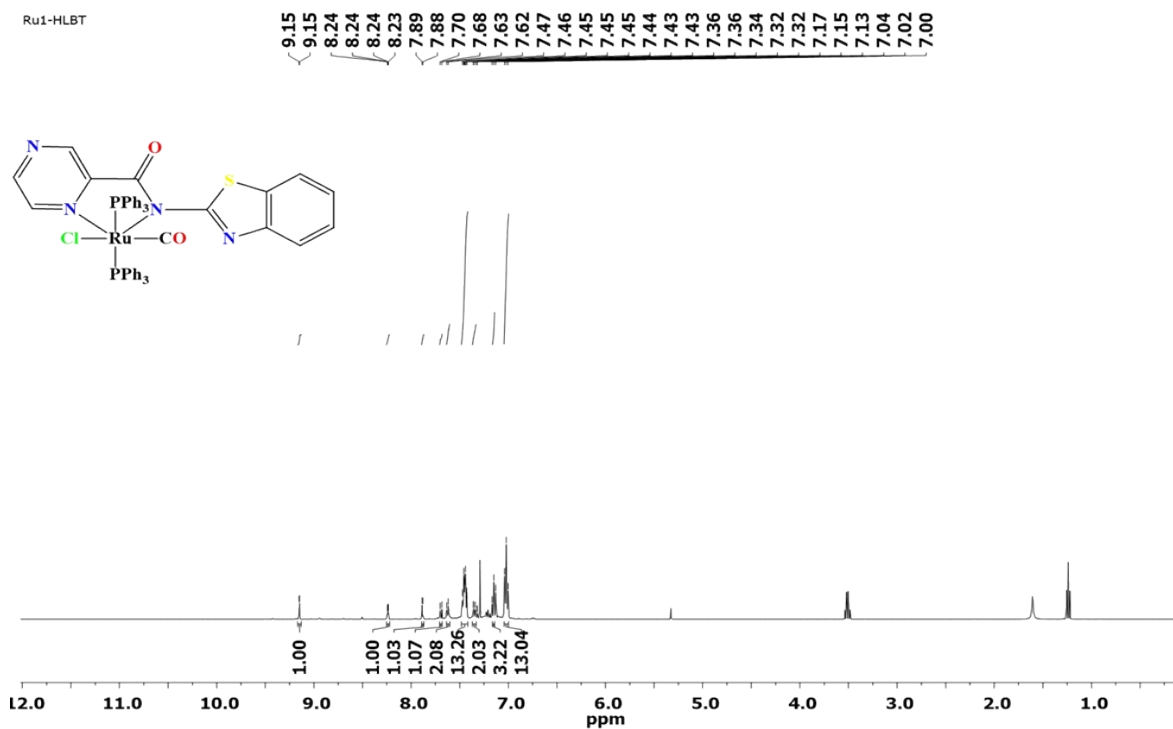


Figure S3. ^1H NMR spectrum (400 MHz, 298K d - CDCl_3) of complex, **Ru1** showing the signature peak ($\text{H}_{\text{pyrazine}}$) shifting from δ_{H} : 9.37 to δ 9.15 ppm upfield.

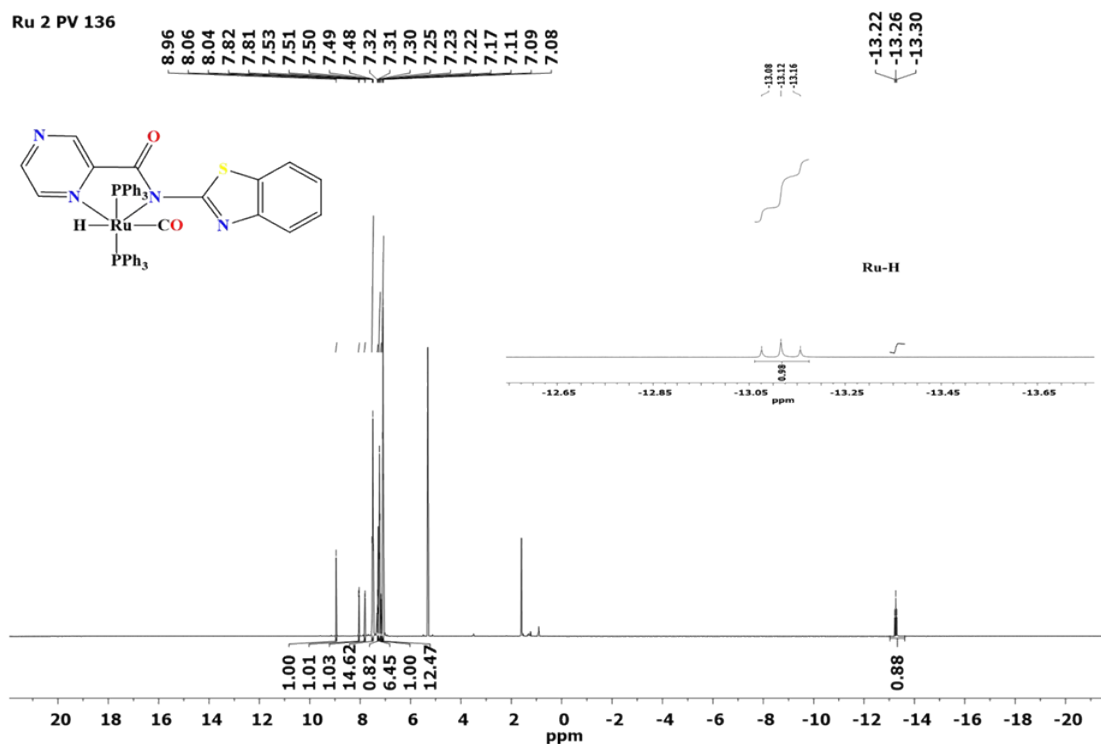


Figure S4. ^1H NMR spectrum (400 MHz, 298K $d\text{-CDCl}_3$) of complex **Ru2** showing triplet peak of co-ligand (H-) ranging between δ_{H} : -13.08-13.16 ppm.

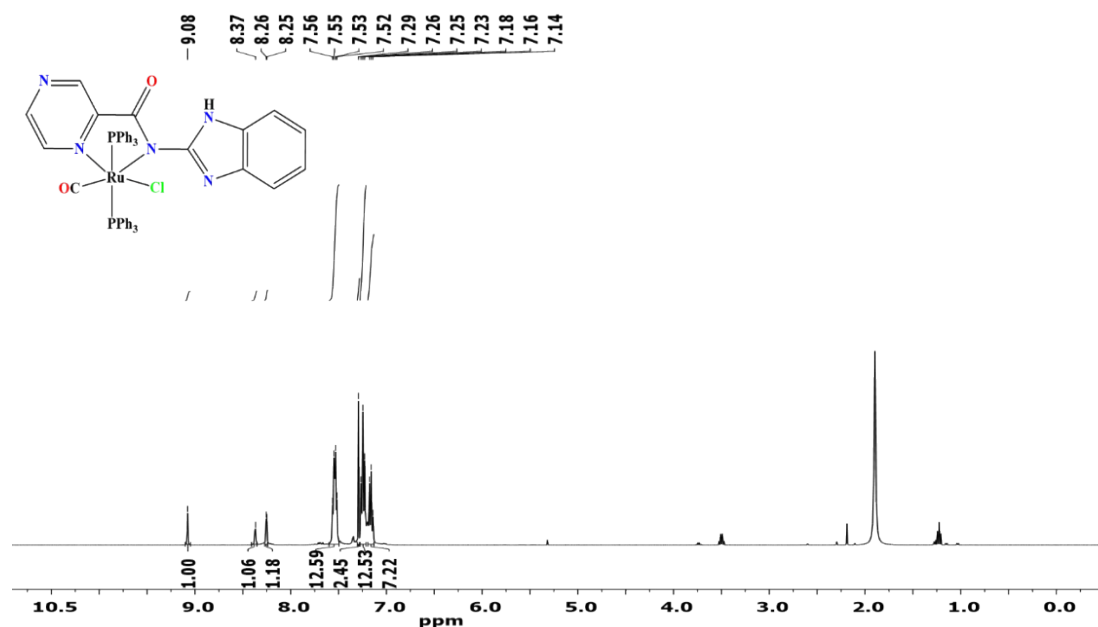


Figure S5. ^1H NMR spectrum (400 MHz, 298K $d\text{-CDCl}_3$) of complex **Ru3** indicating shift of signals corresponding to $\text{H}_{\text{N-H}}$ (δ_{H} : 12.20 to 11.89 ppm) and $\text{H}_{\text{pyrazine}}$ (δ_{H} : 9.37 to 9.08 ppm) which confirm successful coordination.

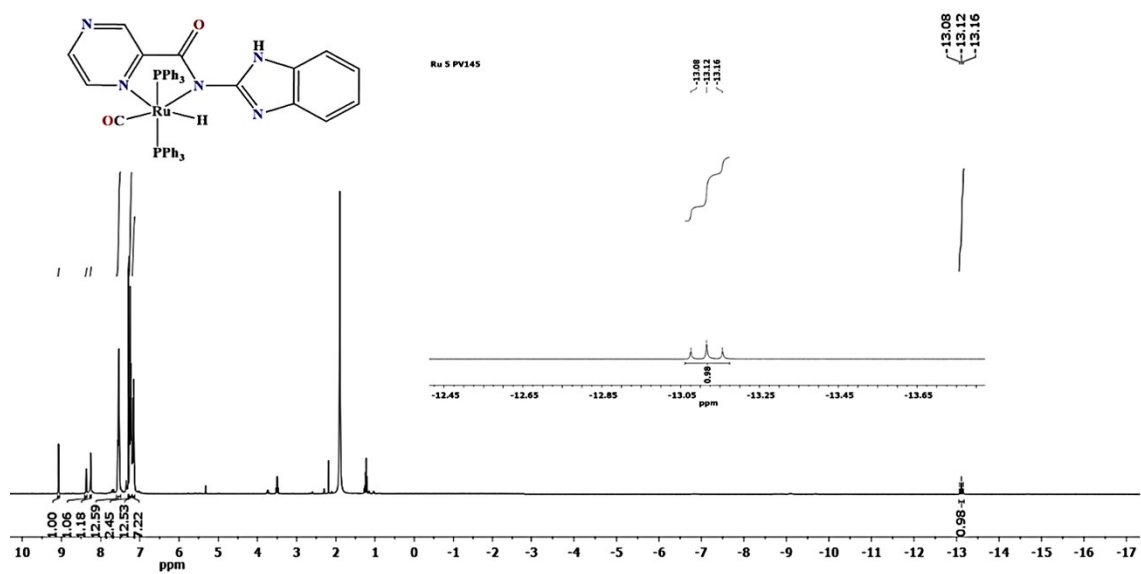


Figure S6. ^1H NMR spectrum (400 MHz, 298K $d\text{-CDCl}_3$) of complex **Ru4** indicating triplet peak of co-ligand (H^-) ranging between δ_{H} : -13.08-13.16 ppm and shifts in $\text{H}_{\text{pyrazine}}$ (from δ_{H} : 9.20 to 9.24 ppm) and $\text{H}_{\text{N-H}}$ (from δ_{H} : 12.08 to 12.02 ppm) proton signals confirming formation the compound.

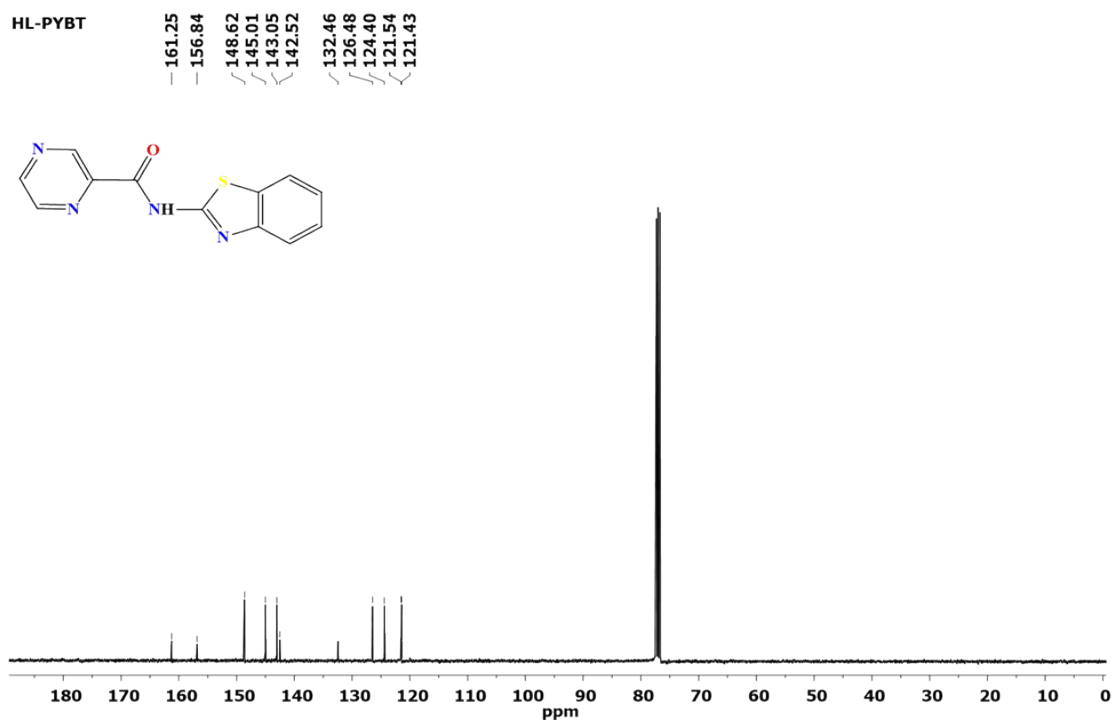


Figure S7. $^{13}\text{C}\{^1\text{H}\}$ NMR spectrum (100 MHz, 298K $d\text{-CDCl}_3$) of *N*-(benzo[d]thiazol-2-yl)pyrazine-2-carboxamide ligand, **HL1** showing the C=O signal at δ : 161.3 ppm confirming the successful formation of the ligands.

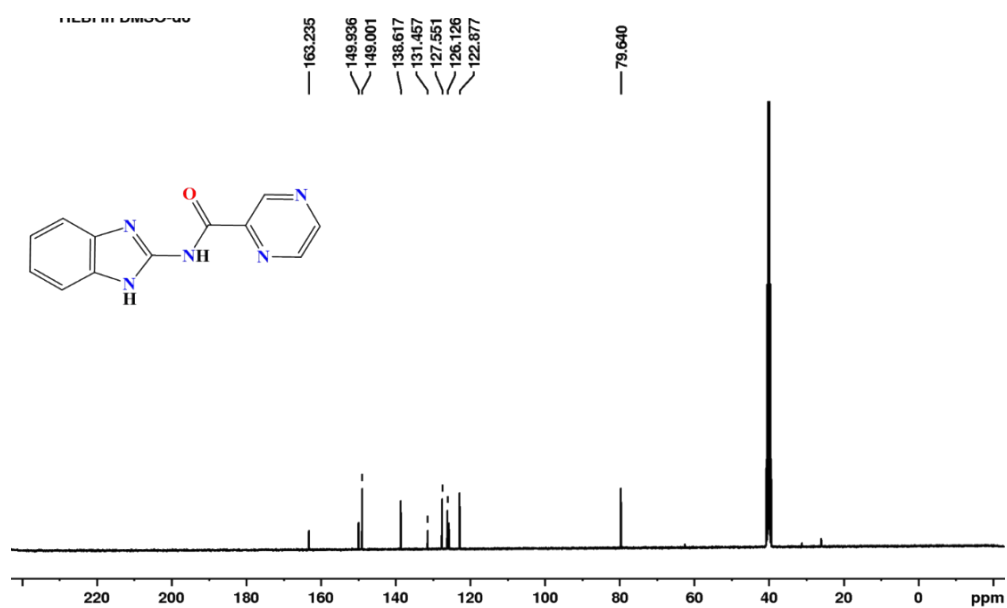


Figure S8. $^{13}\text{C}\{^1\text{H}\}$ NMR spectrum of *N*-(1*H*-benzo[d]imidazol-2-yl)pyrazine-2-carboxamide ligand, **HL2** showing the C=O signal at δ : 161.3 ppm confirming the successful formation of the ligands.

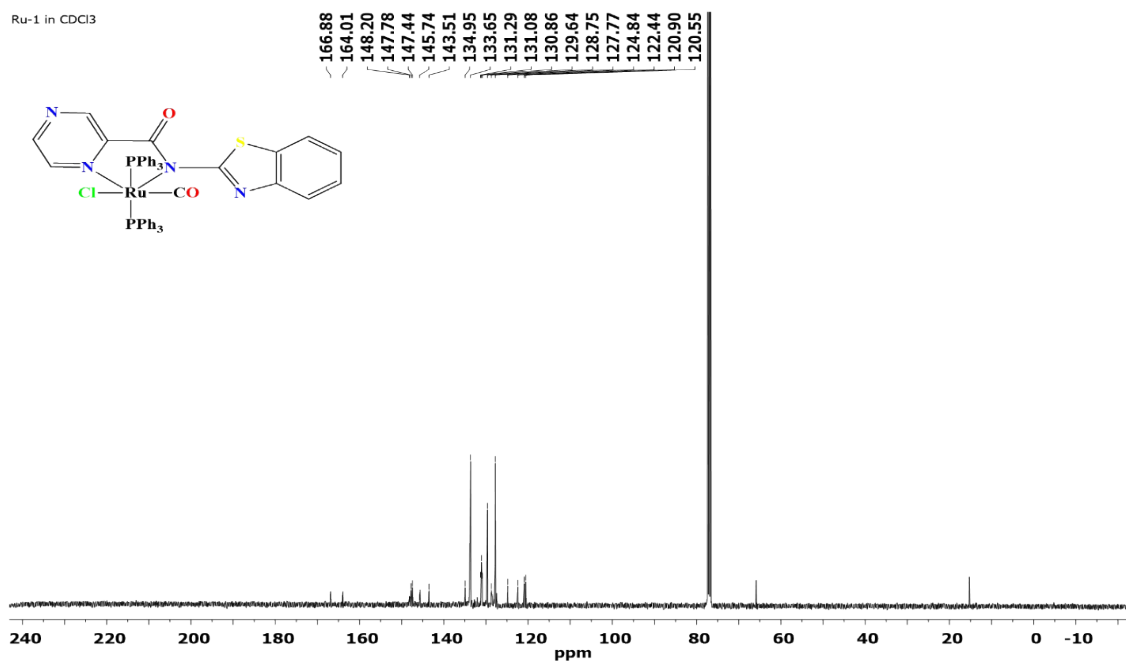


Figure S9. $^{13}\text{C}\{^1\text{H}\}$ NMR spectrum (100 MHz, 298K *d.* CDCl_3) of complex **Ru1** showing signal at $\delta=166.88$ ppm corresponding to the C=O signal confirming the successful coordination.

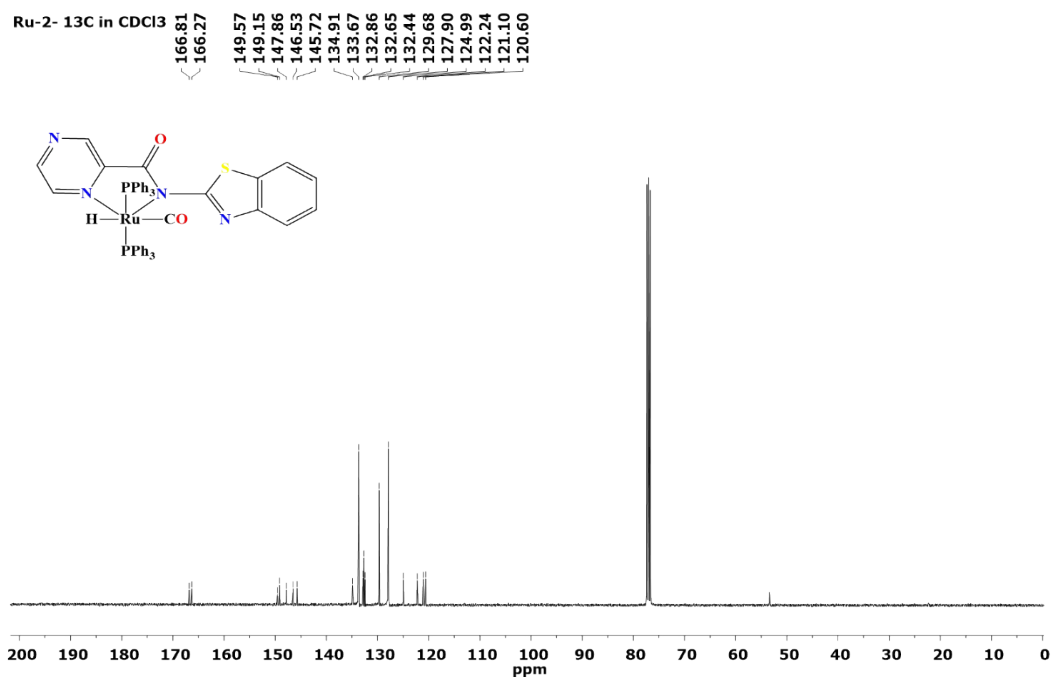


Figure S10. $^{13}\text{C}\{^1\text{H}\}$ NMR spectrum (100 MHz, 298K $d\text{-CDCl}_3$) of complex **Ru2** indicating a shift in the chemical shift of C=O (δ : 166.81 ppm) downfield upon coordination.

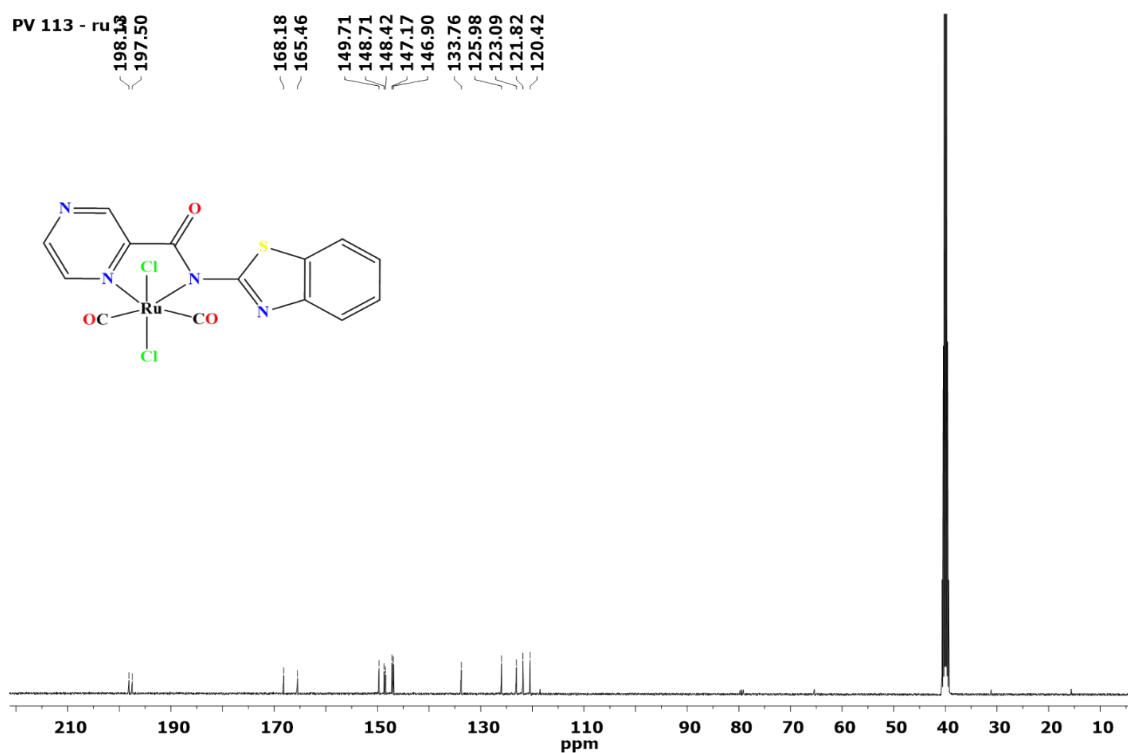


Figure S11. $^{13}\text{C}\{^1\text{H}\}$ NMR spectrum (100 MHz, 298K $d\text{-CDCl}_3$) of complex **Ru3** indicating a shift in the chemical shift of C=O (δ : 166.81 ppm) downfield upon coordination.

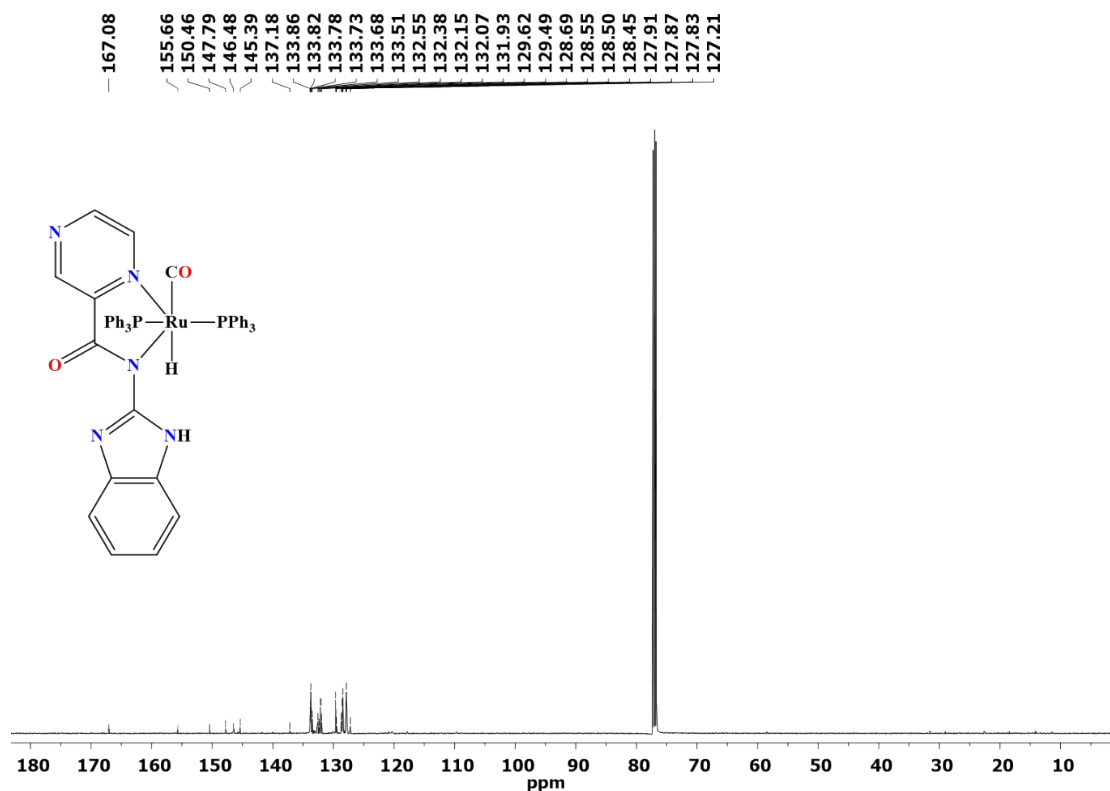


Figure S12. $^{13}\text{C}\{^1\text{H}\}$ NMR spectrum (100 MHz, 298K $d\text{-CDCl}_3$) of complex **Ru4** indicating a shift in the chemical shift of C=O (δ : 166.81 ppm) downfield upon coordination.

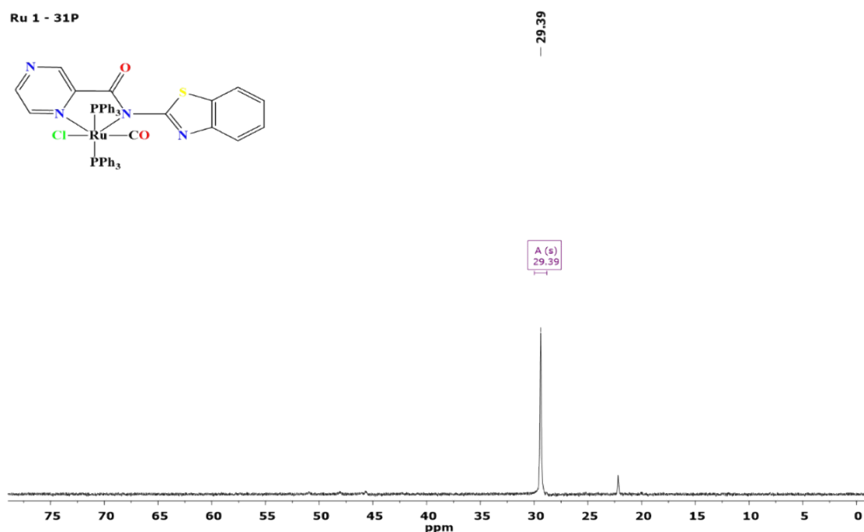


Figure S13. $^{31}\text{P}\{^1\text{H}\}$ NMR spectrum (100 MHz, 298K $d_6\text{ CDCl}_3$) of complex **Ru1** indicating a signal corresponding to two equivalent PPh_3 *trans* to each other.

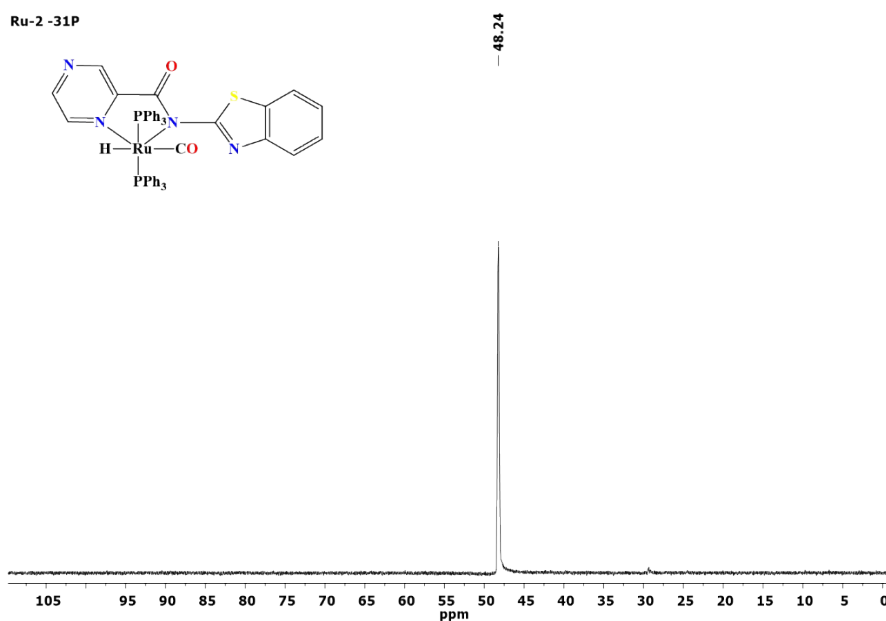


Figure S14. $^{31}\text{P}\{^1\text{H}\}$ NMR spectrum of (100 MHz, 298K d_6 CDCl_3) complex **Ru2** indicating a signal corresponding to two equivalent PPh_3 *trans* to each other.

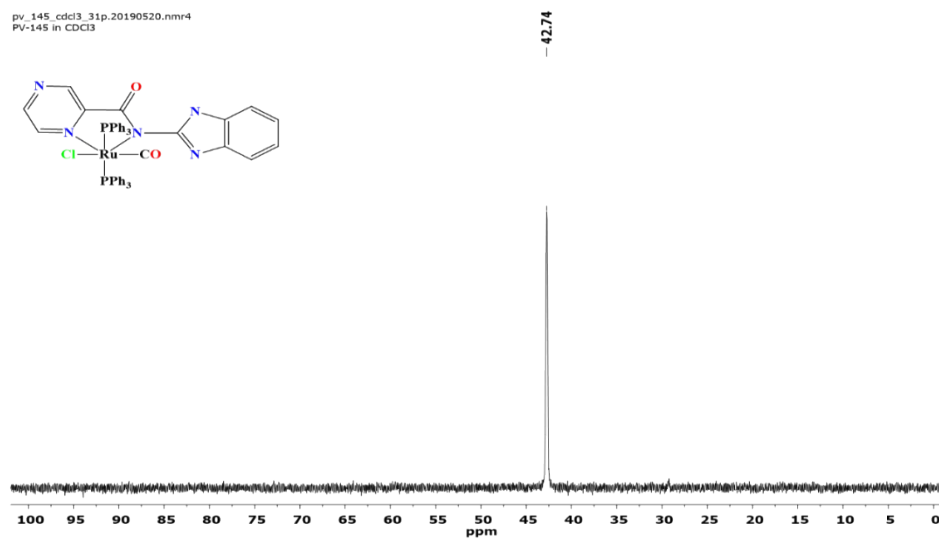


Figure S15. $^{31}\text{P}\{^1\text{H}\}$ NMR spectrum (100 MHz, 298K d_6 CDCl_3) of complex **Ru3** showing a signal at δ : 42.74 ppm confirming to two equivalent PPh_3 *trans* to each other.

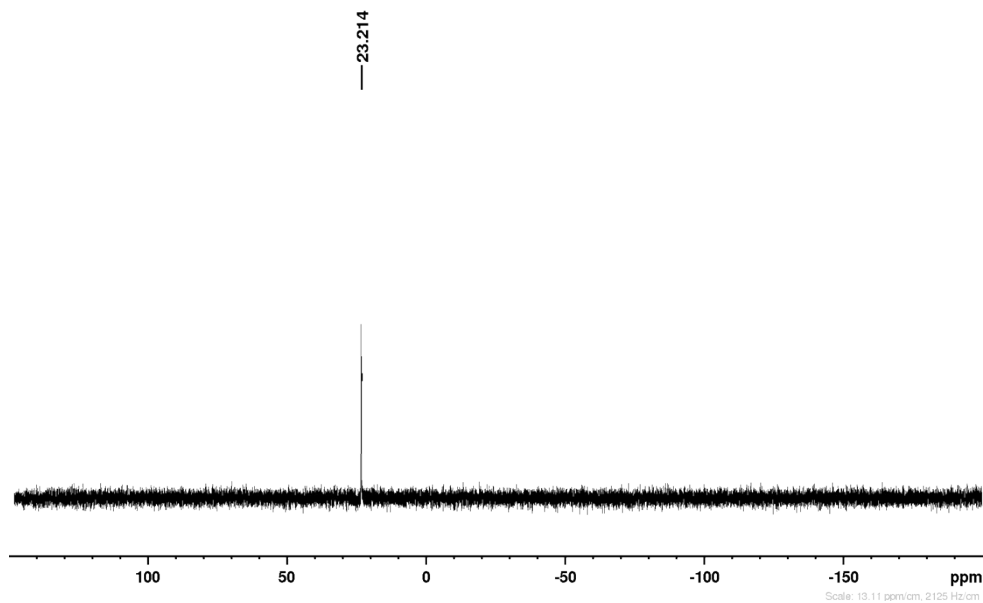


Figure S16. $^{31}\text{P}\{^1\text{H}\}$ NMR spectrum (122 MHz, 298K $d\text{-CDCl}_3$) of complex **Ru4** showing a signal at δ : 48.33 ppm implicating presence of two equivalent PPh_3 *trans* to each other.

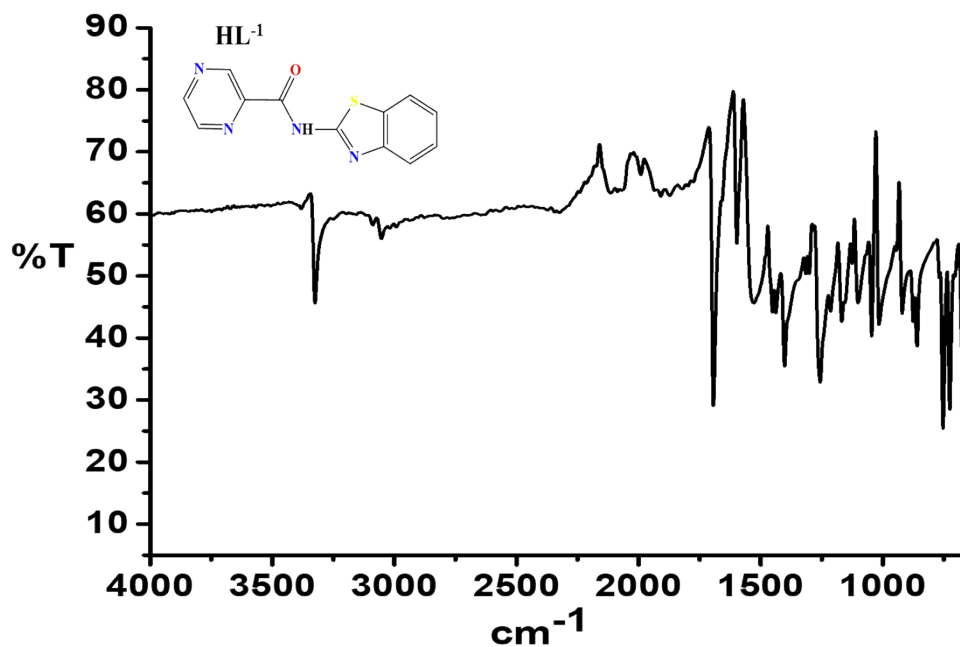


Figure S17. FT-IR spectrum of *N*-(benzo[*d*]thiazol-2-yl)pyrazine-2-carboxamide ligand, **HL1** showing its characteristic signals of $\nu(\text{N-H})$: 3324 cm^{-1} , 1691; $\nu(\text{C=O})$: 1691 cm^{-1} ; 1543 $\nu(\text{C=N})$:

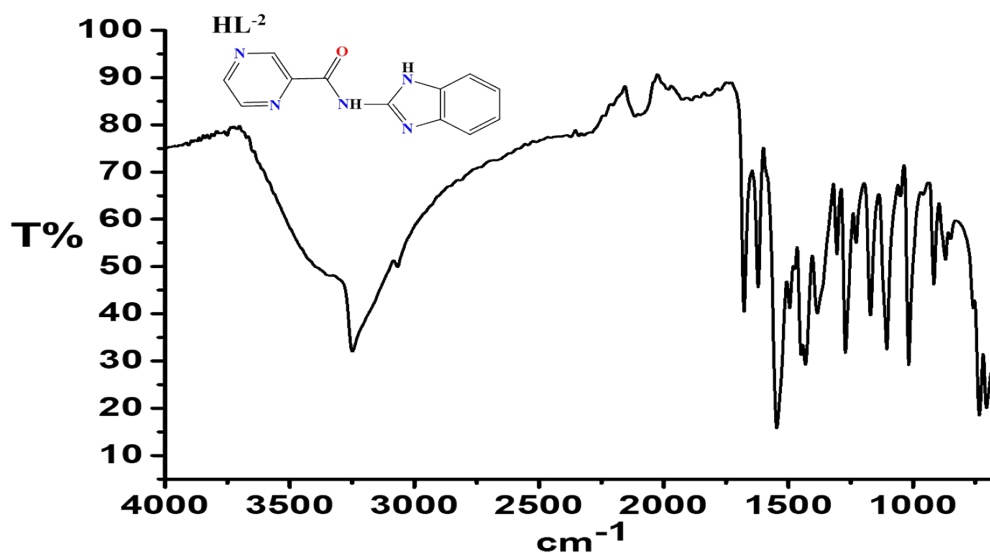


Figure S18. FT-IR spectrum of *N*-(benzo[d]imidazol-2-yl)pyrazine-2-carboxamide ligand, **HL2** depicting the characteristic signals of $\nu(\text{N-H})$: 3251 cm^{-1} , $\nu(\text{C=O})$: 1684 cm^{-1} , 1546 cm^{-1} $\nu(\text{C=N})$.

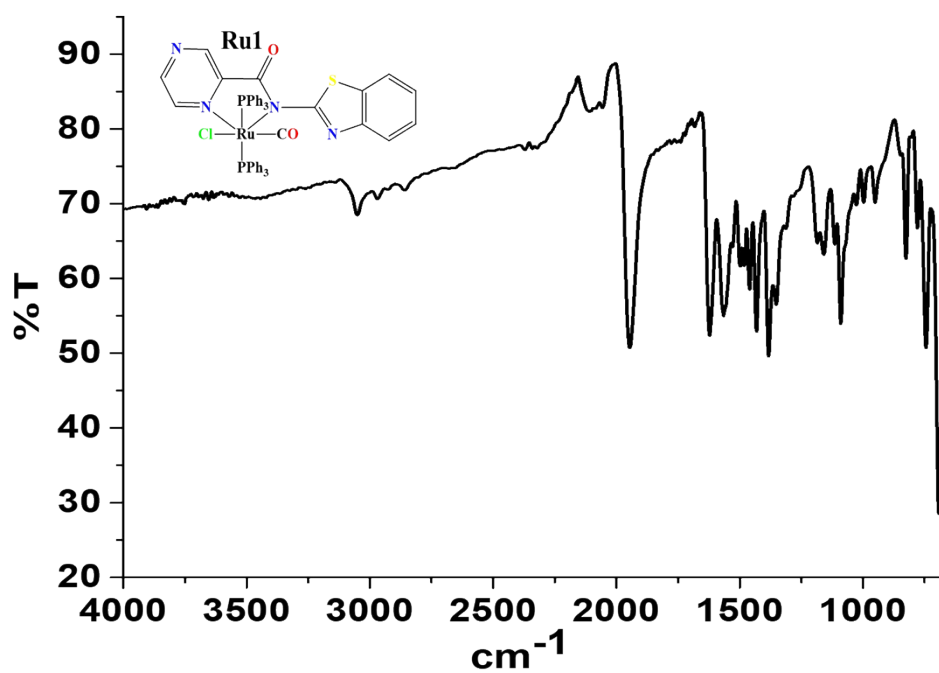


Figure S19. FT-IR spectrum of complex **Ru1** depicting signature signals at: 1935 cm^{-1} , $\nu\text{C}\equiv\text{O}$: and 1629 cm^{-1} , 1565 cm^{-1} $\nu(\text{C=N})$.

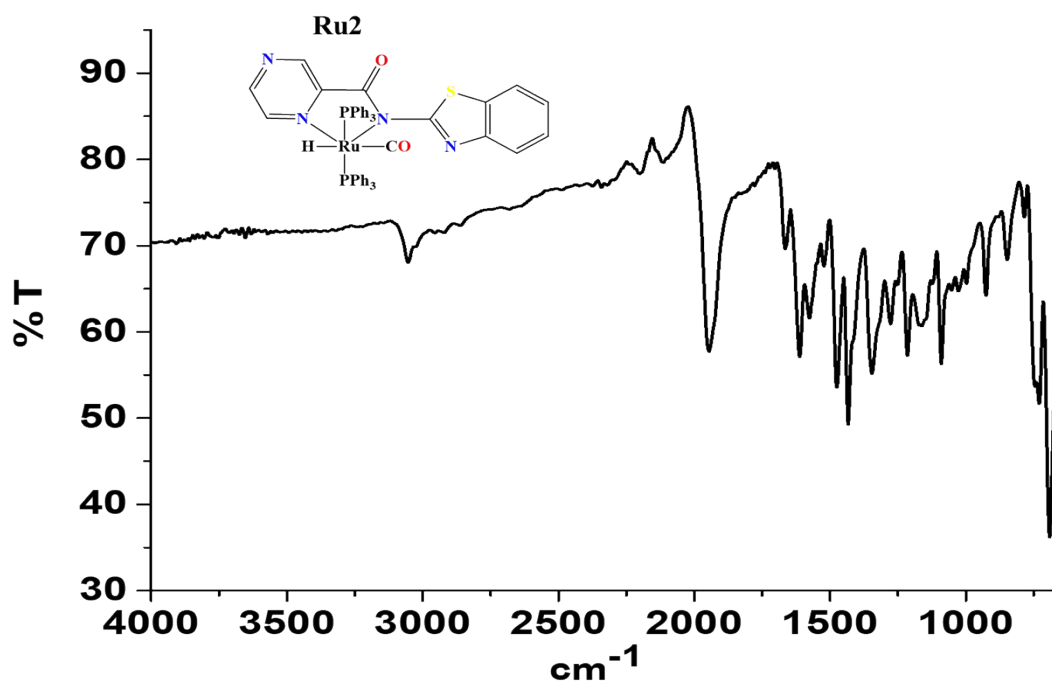


Figure S20. FT-IR spectrum of complex **Ru2** depicting signature signals: 1935 cm^{-1} $\nu(\text{C}\equiv\text{O})$; 1626 cm^{-1} , $\nu(\text{C}=\text{O})$; 1567 cm^{-1} $\nu(\text{C}=\text{N})$.

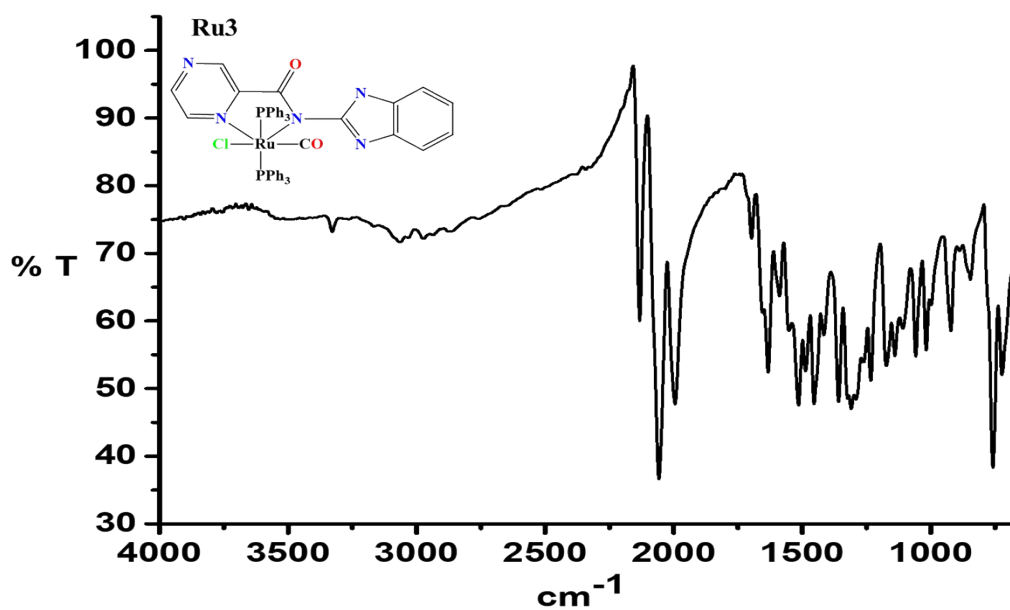


Figure S21. FT-IR spectrum of complex **Ru3** depicting signature signals at: 1947 cm^{-1} $\nu(\text{C}\equiv\text{O})$; 1622 cm^{-1} $\nu(\text{C}=\text{O})$; and 1562 cm^{-1} $\nu(\text{C}=\text{N})$.

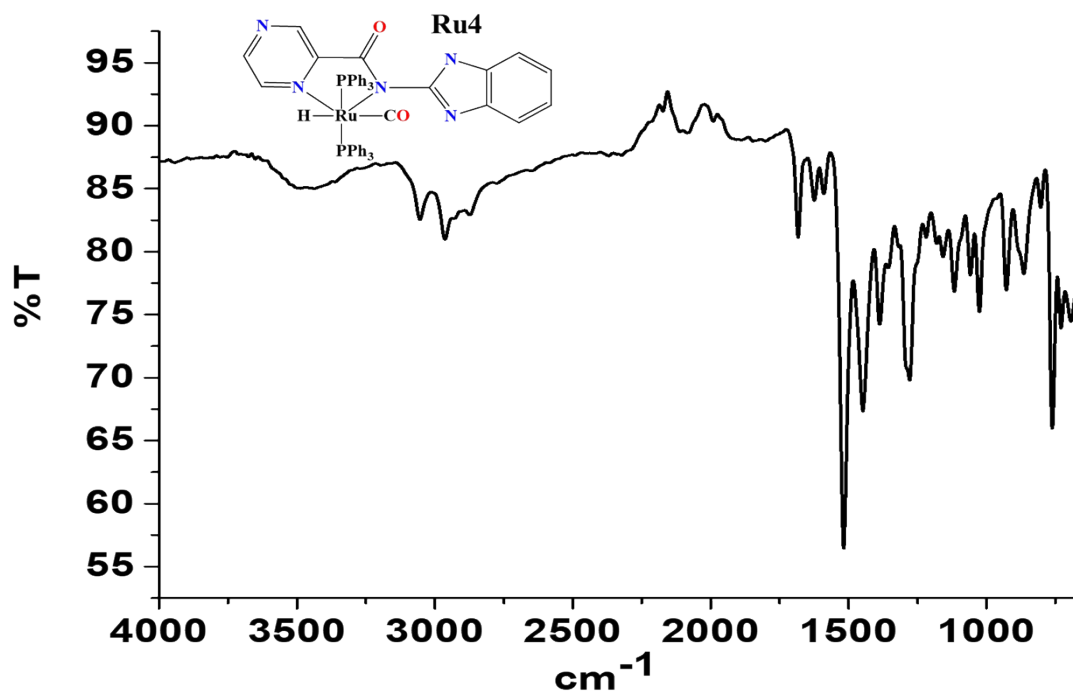


Figure S22. FT-IR spectrum of complex **Ru4** depicting signature signals at 1946 cm^{-1} $\nu(\text{C}\equiv\text{O})$; 1612 cm^{-1} $\nu(\text{C}=\text{O})$; and 1569 cm^{-1} $\nu(\text{C}=\text{N})$.

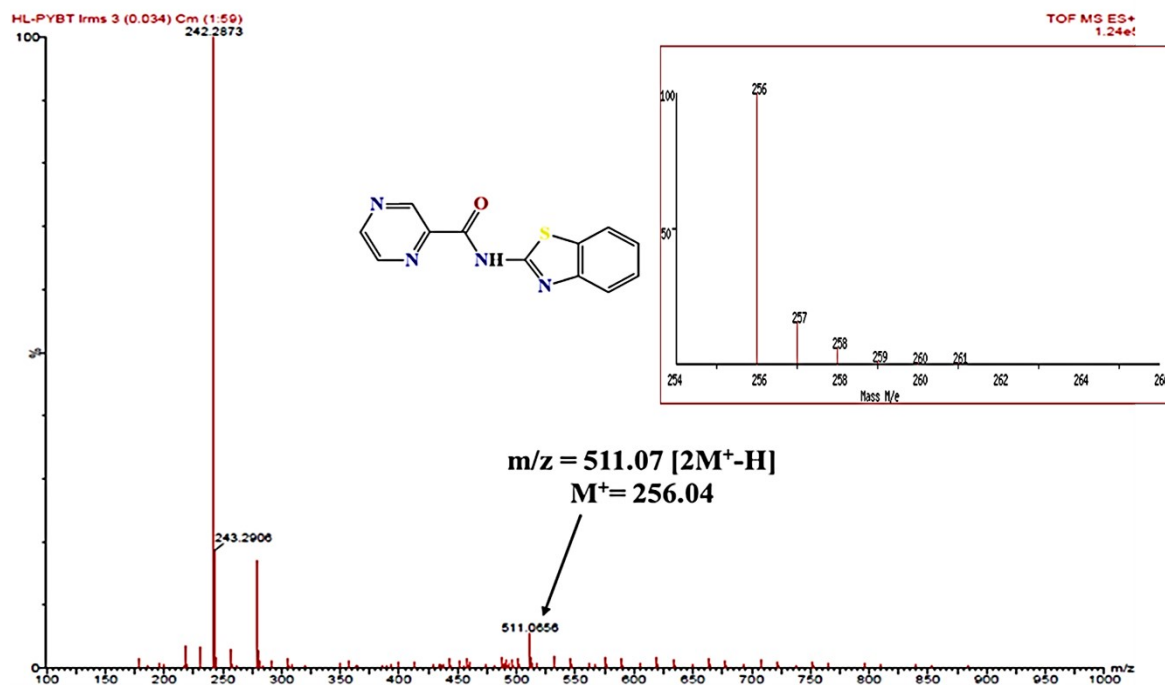


Figure S23. LR MS spectrum (positive ion mode) of **HL1** indicating dimeric form of the ligand at $m/z = 511.07$. The theoretical isotopic mass distribution plot (inset).

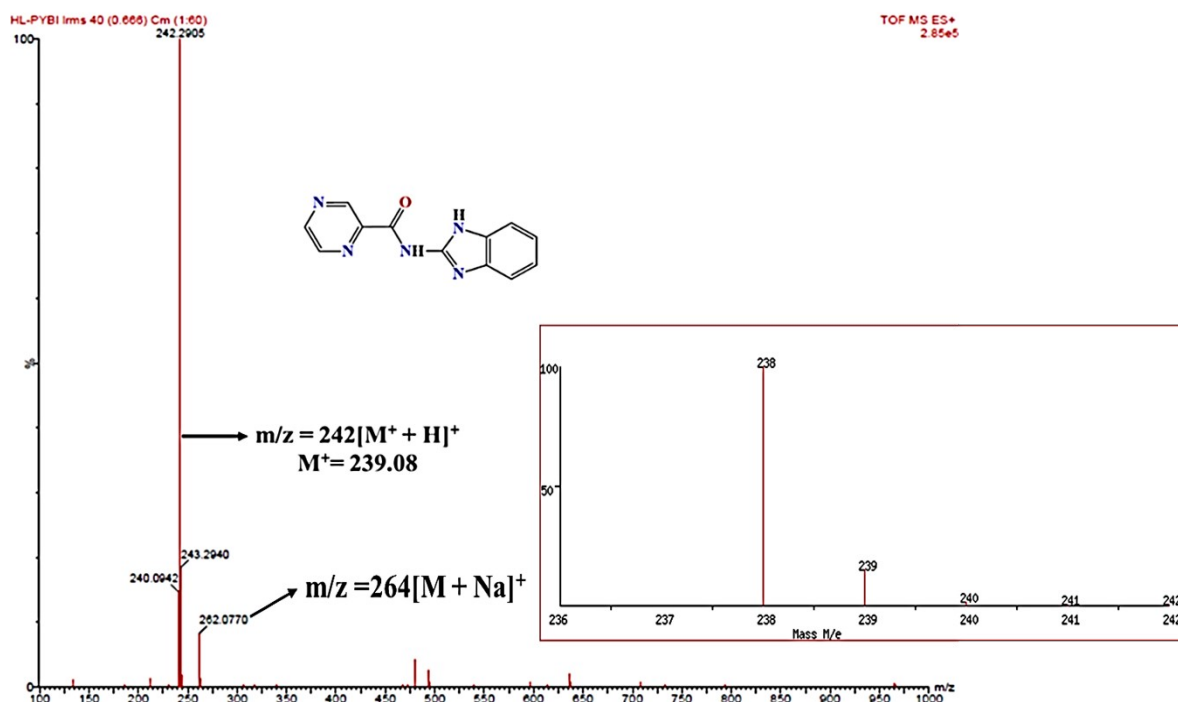


Figure S24. LR MS spectrum (positive ion mode) of **HL2** depicting a peak at $m/z = 242$ corresponding to $[M + H]^+$. The theoretical isotopic mass distribution plot (inset).

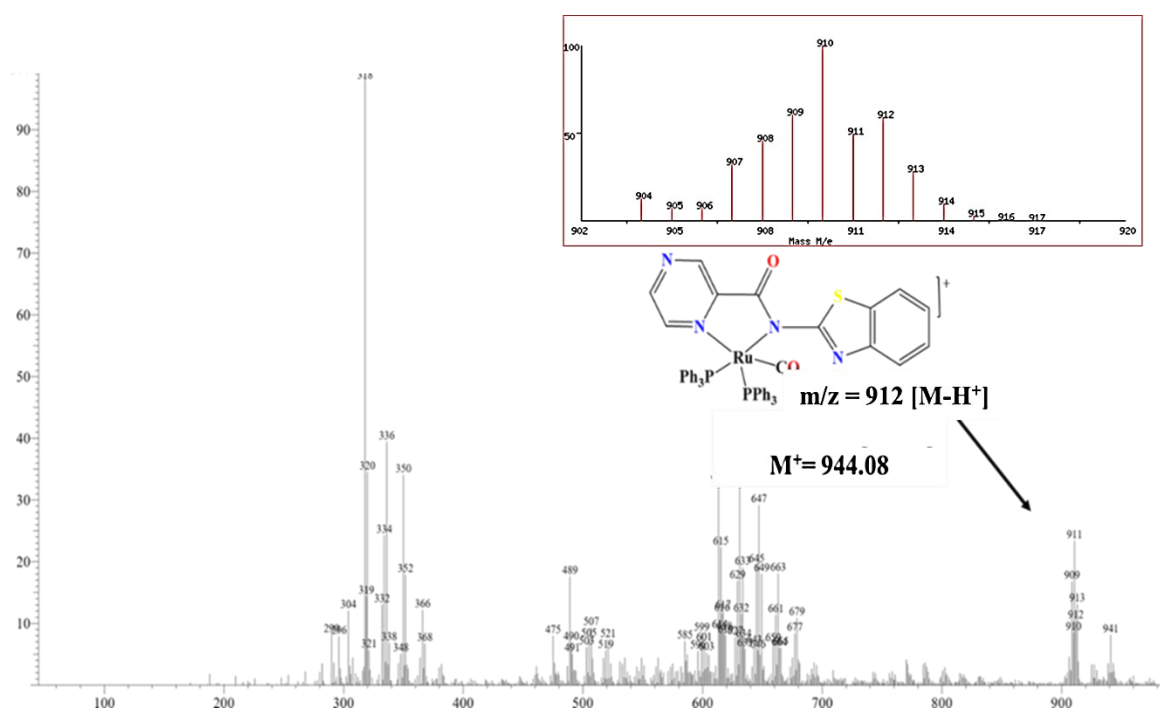


Figure S25. LC-MS spectrum of **Ru1**. The simulated theoretical mass distribution plot (inset).

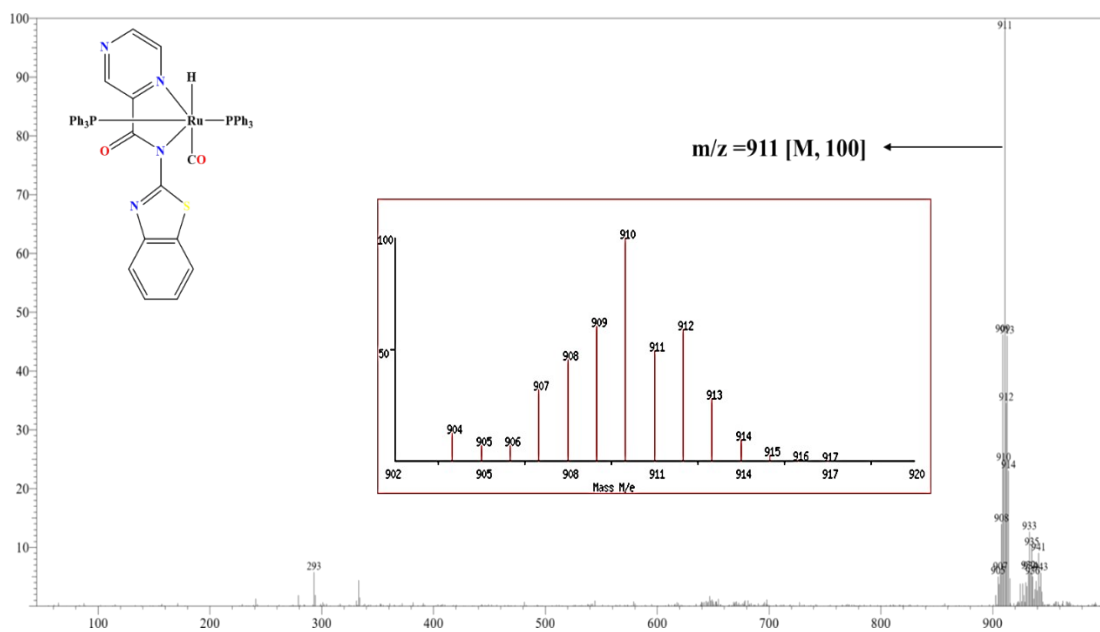


Figure S26. LC-MS spectrum of **Ru2**. The simulated theoretical mass distribution plot (inset).

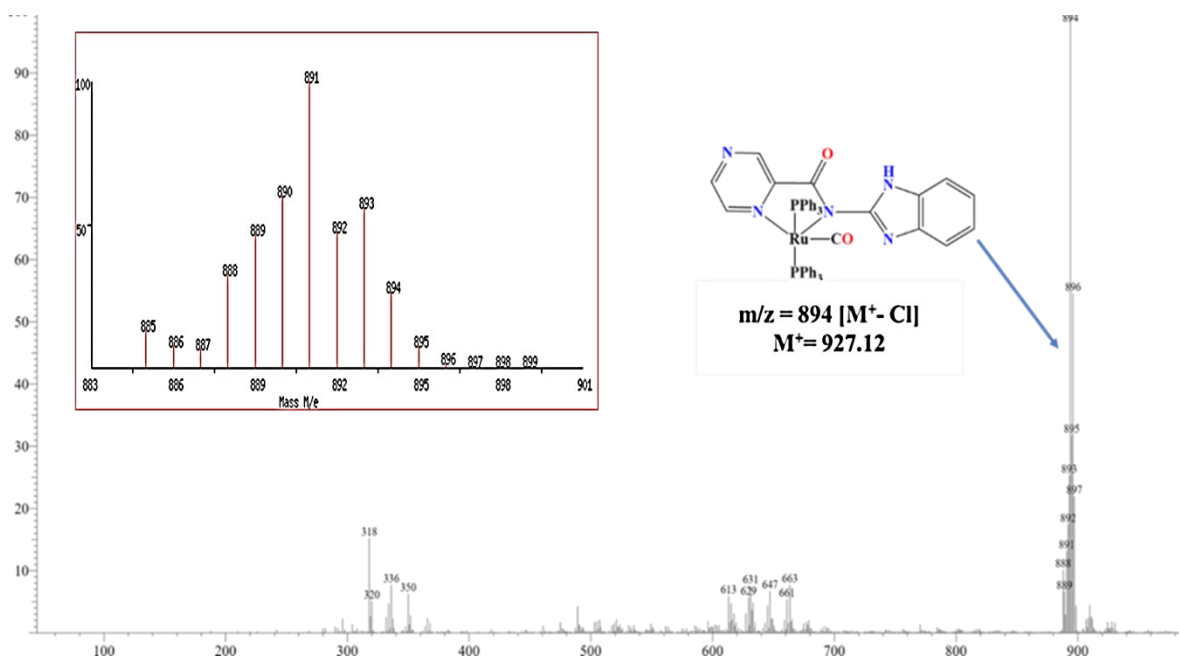


Figure S27. LC-MS spectrum of **Ru3**. The simulated theoretical mass distribution plot (inset).

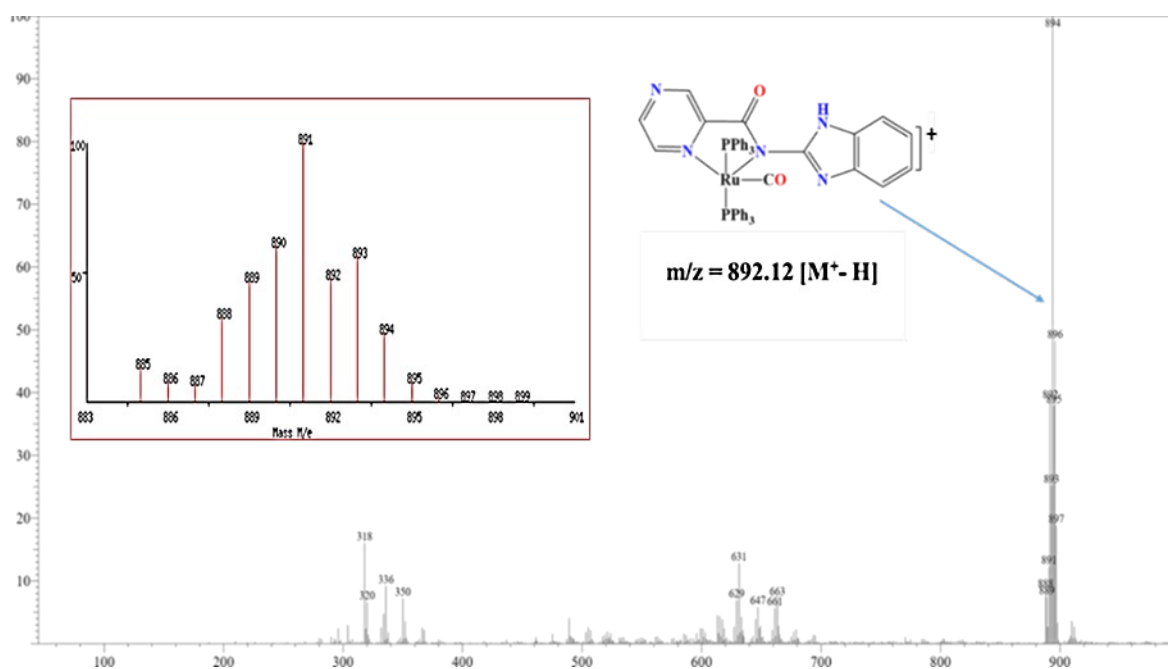


Figure S28. LC-MS spectrum of **Ru4** indicating the molecular mass of the fragment $[M - H]$ at $m/z = 892.12$. Inset is the simulated theoretical mass distribution plot.

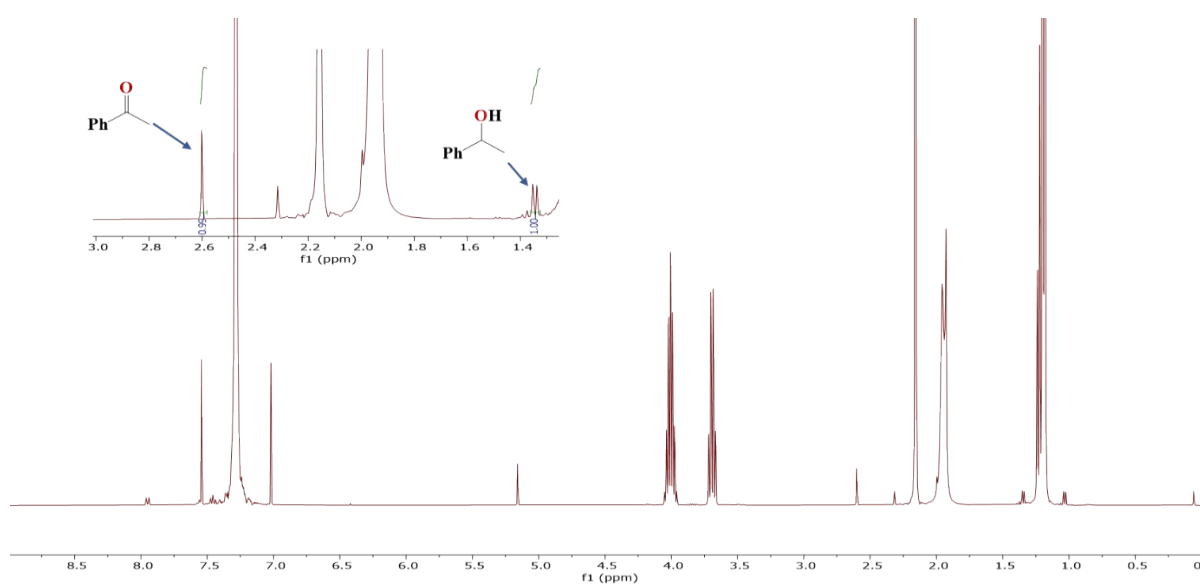


Figure S29. ^1H NMR spectrum (400 MHz, $d\text{-CDCl}_3$) of transfer hydrogenation of acetophenone reaction mixture (**Ru3** was used as catalyst). Aliquot withdrawn and analysed after 4 h of reaction. The integral values of methyl peaks of acetophenone and 1-phenylethanol corresponding to percentage conversions of 50% and yields of 50%.

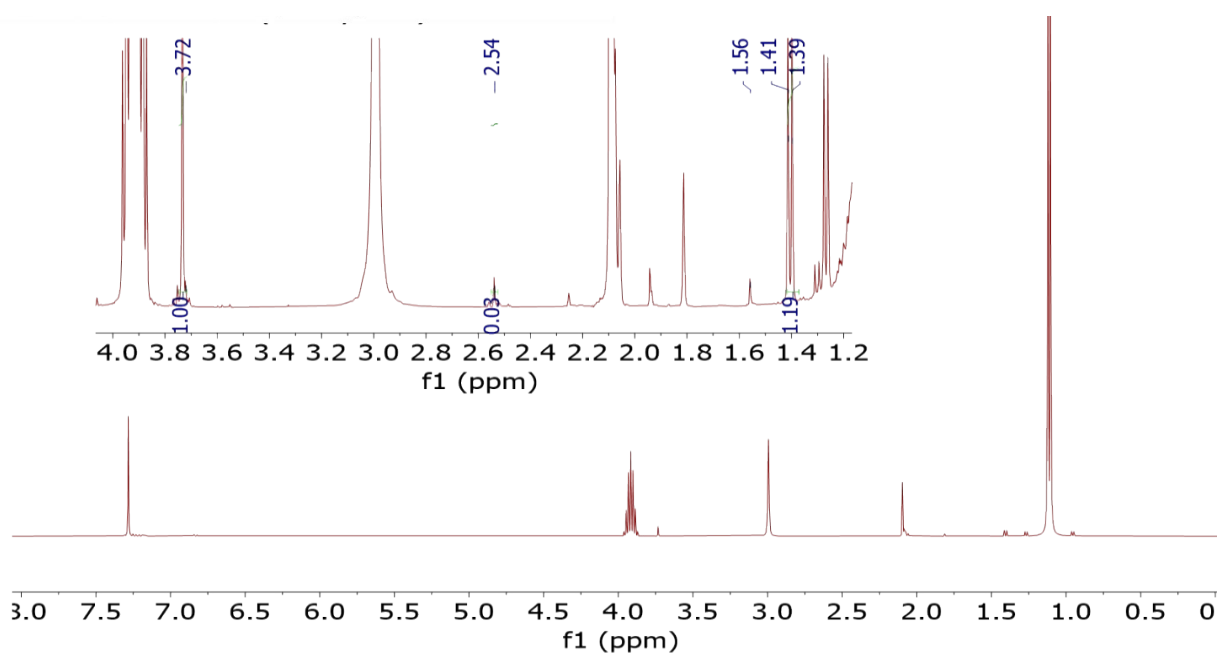


Figure S30. ^1H NMR spectrum (400 MHz, $d\text{-CDCl}_3$) of TH of acetophenone. (**Ru4** was used as catalyst). Aliquot was taken and analysed after 6 h of reaction. The integral values of methyl protons of acetophenone and 1-phenylethanol corresponding to conversion of 97% and Yield of 97%.

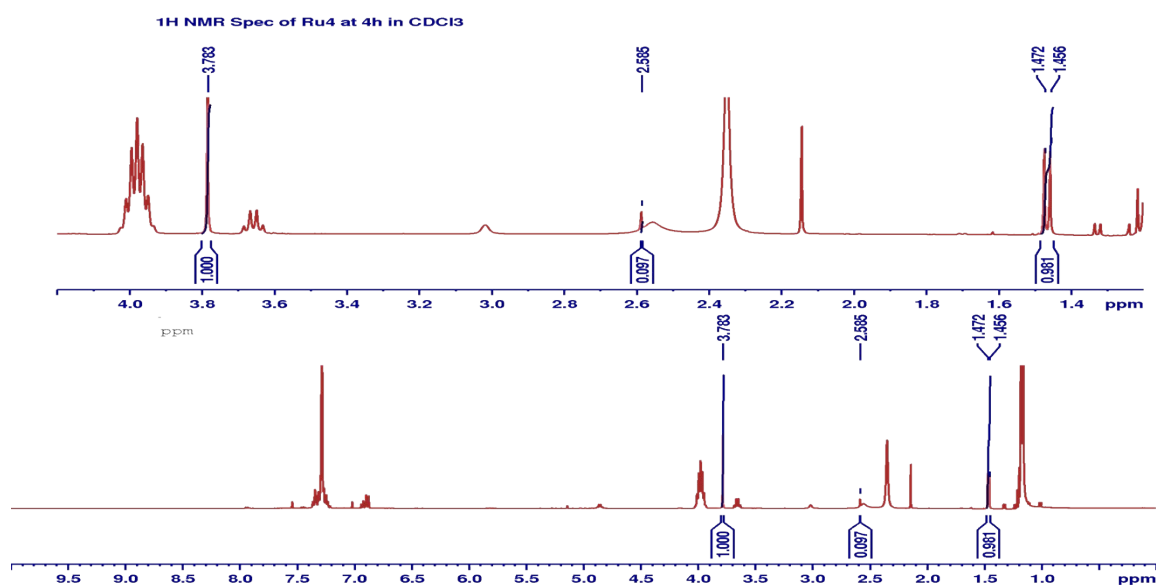


Figure S31. ^1H NMR spectrum (400 MHz, $d\text{-CDCl}_3$) of the reaction of transfer hydrogenation of acetophenone (**Ru4** used as catalyst). Aliquot was taken and analysed after 6 h of reaction. The integral values of methyl protons of acetophenone and 1-phenylethanol correspond to conversion of 91% and yield of 90%.

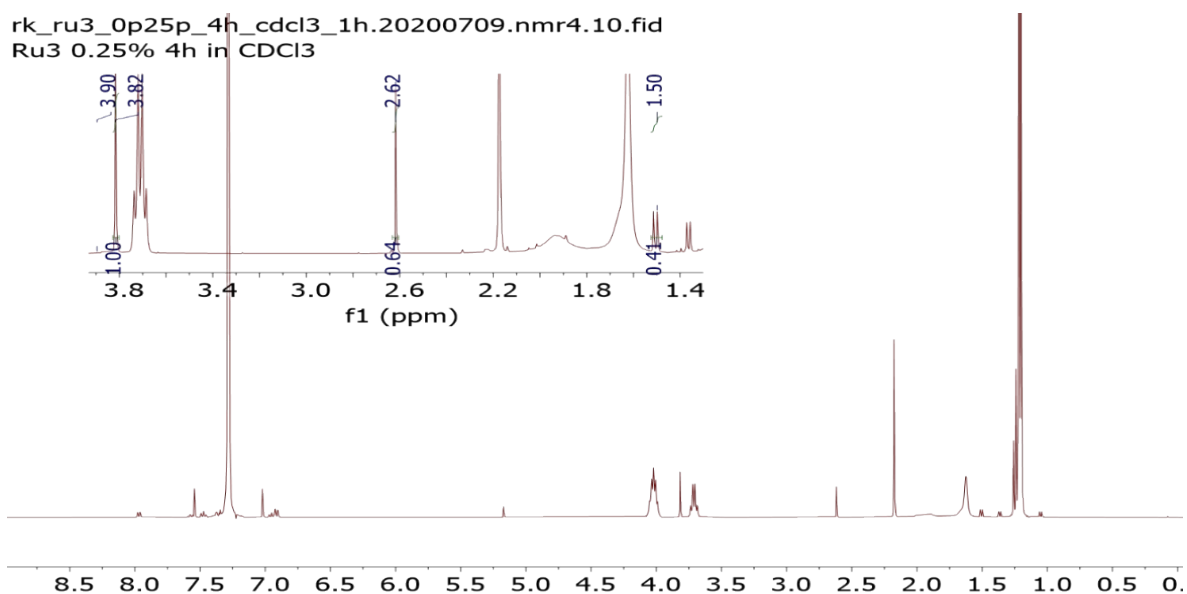


Figure S32. ^1H NMR spectrum (400 MHz, $d\text{-CDCl}_3$) of the reaction of transfer hydrogenation of acetophenone (**Ru3**:catalyst loading of 0.25 mol%). Aliquot sampled and analysed after 4 h of reaction. The integral values of the methyl protons of acetophenone and 1-phenylethanol correspond to percentage conversion of 46% and yield of 41%.

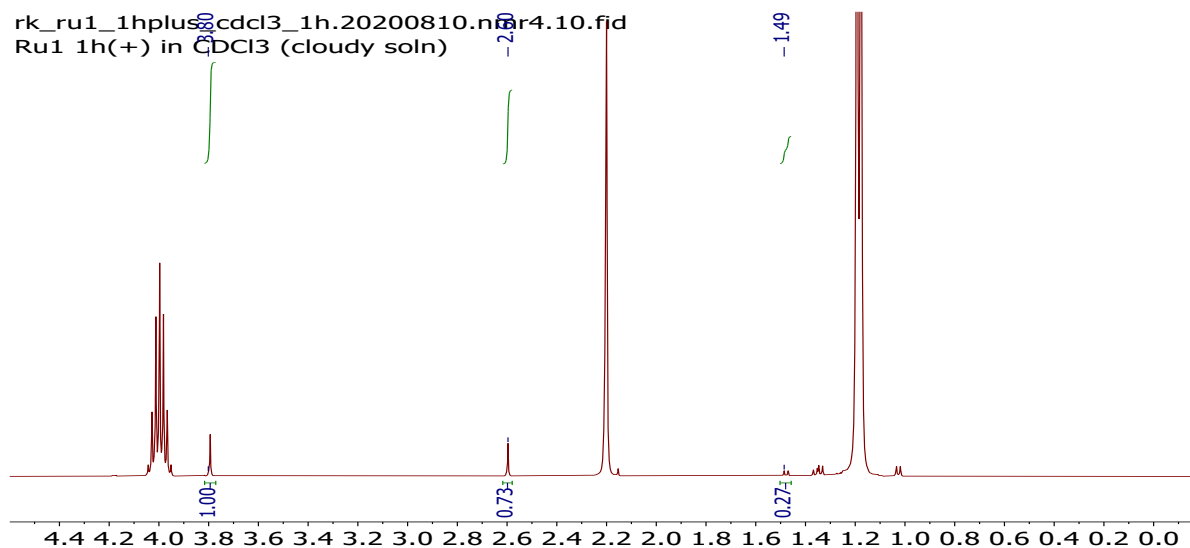


Figure S33. ^1H NMR spectrum (400 MHz, $d\text{-CDCl}_3$) of the reaction of transfer hydrogenation of acetophenone (**Ru1**: catalyst loading of 0.25 mol%). Aliquot was sampled and analysed after 1 h of reaction. The integral values of the methyl protons of acetophenone and 1-phenylethanol correspond to the percentage conversion of 27% and yield of 27% (Figure S47).

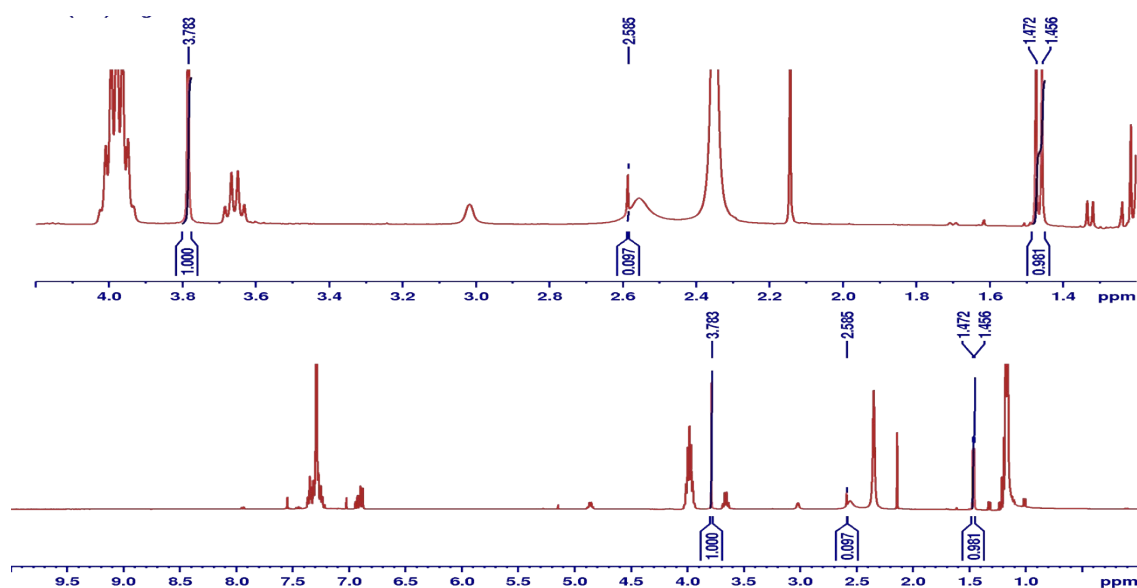


Figure S34. ^1H NMR spectrum (400 MHz, $d\text{-CDCl}_3$) of transfer hydrogenation of 4-chloroacetophenone reaction mixture (**Ru4** used as catalyst). Aliquot taken and analysed after at 4h reaction. The integral values of the methyl protons of 4-chloroacetophenone and 4-chlorophenylethanol correspond to the percentage conversion of 98% and yield of 98% (Table 4, entry 3).

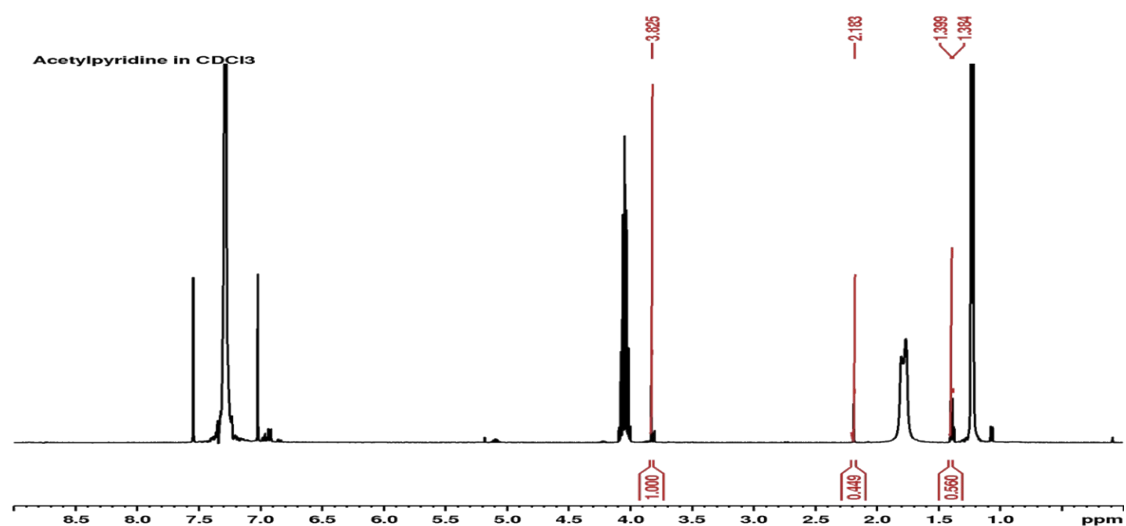


Figure S35. ^1H NMR spectrum (400 MHz, $d\text{-CDCl}_3$) of transfer hydrogenation of 2-acetylpyridine reaction mixture (**Ru4** used as catalyst). Aliquot taken and analysed after at 4h reaction. The integral values of the methyl protons of 2-acetylpyridine and product correspond to the percentage conversion of 55% and yield of 55% (Table 4, entry 11).

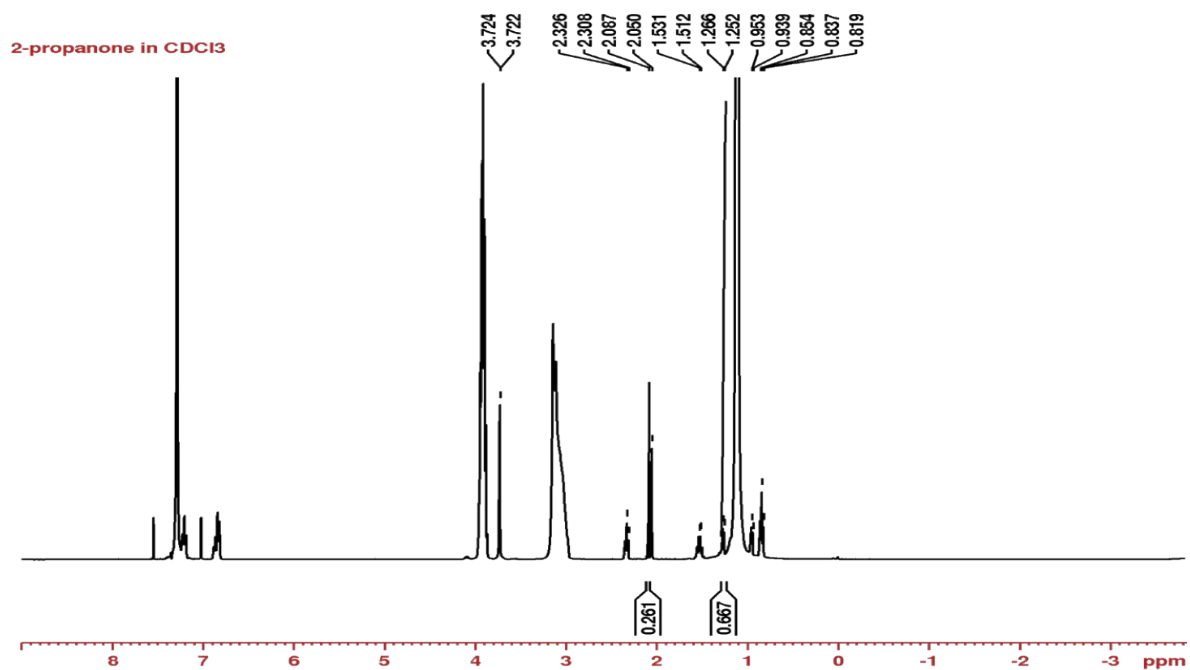


Figure S36. ¹H NMR spectrum (400 MHz, *d*-CDCl₃) of transfer hydrogenation of 2-propanone reaction mixture (**Ru4** used as catalyst). Aliquot taken and analysed after at 4h reaction. The integral values of the methyl protons of 2-propanone and 2-propanol correspond to the percentage conversion of 71% and yield of 71% (Table 4, entry 11).

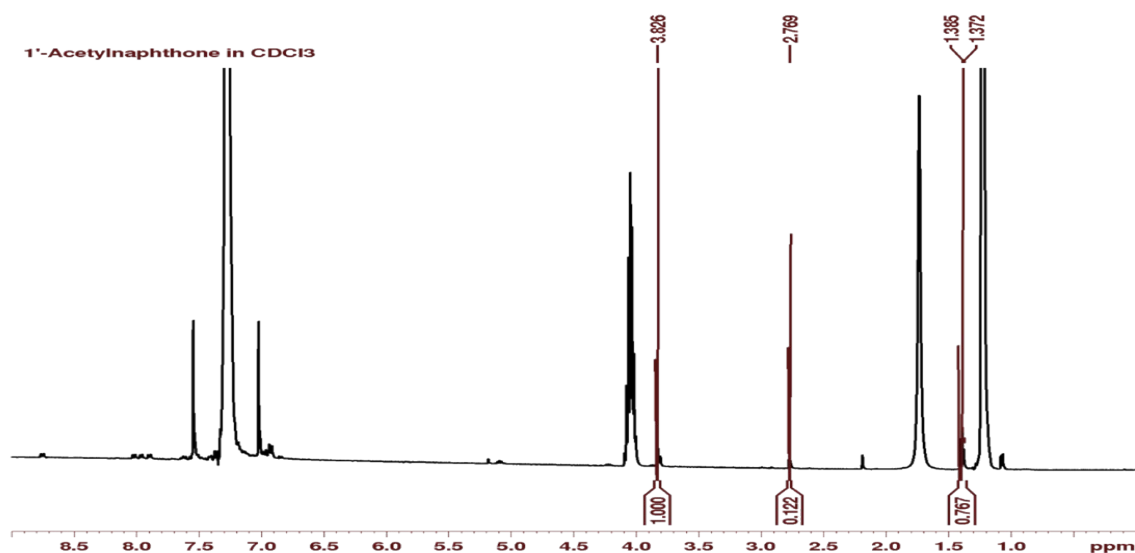


Figure S37. ¹H NMR spectrum (400 MHz, *d*-CDCl₃) of transfer hydrogenation of 1-acetylnaphthone reaction mixture (**Ru4** used as catalyst). Aliquot taken and analysed after at 6h reaction. The integral values of the methyl protons of 1-acetylnaphthone and product correspond to the percentage conversion of 86% and yield of 84% (Table 4, entry 9).

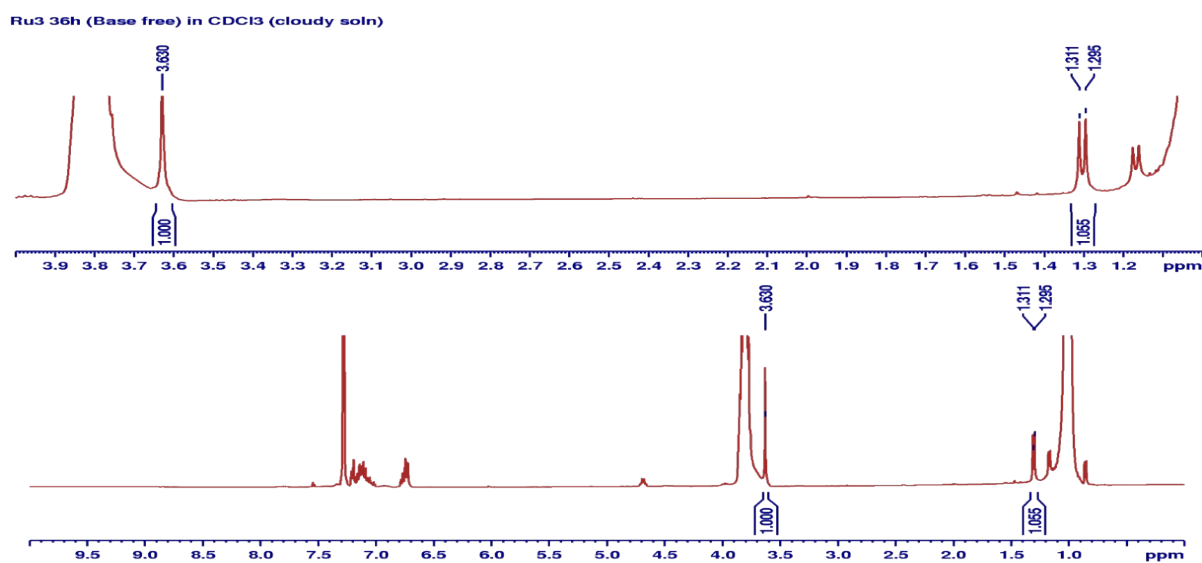


Figure S38. ¹H NMR spectrum (400 MHz, *d*-CDCl₃) of transfer hydrogenation of acetophenone reaction catalysed by **Ru3** without a base. Aliquot taken and analysed after at 36 h of reaction. The integral values of the methyl protons of 1-acetylnaphthone and product correspond to the percentage conversion of 99% and yield of 99% (Table 2, entry 5).

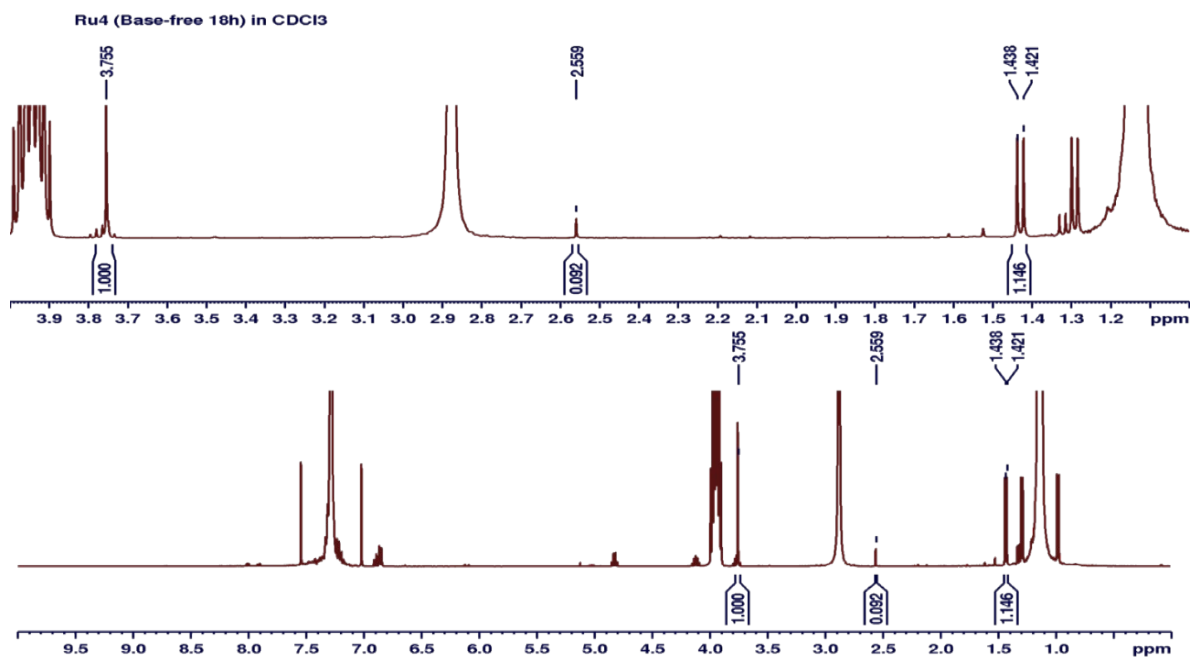


Figure S39. ¹H NMR spectrum (400 MHz, *d*-CDCl₃) of transfer hydrogenation of acetophenone reaction catalysed by **Ru4** without a base. Aliquot taken and analysed after at 18 h of reaction. The integral values of the methyl protons of 1-acetylnaphthone and product correspond to the percentage conversion of 93% and yield of 93% (Table 2, entry 4).

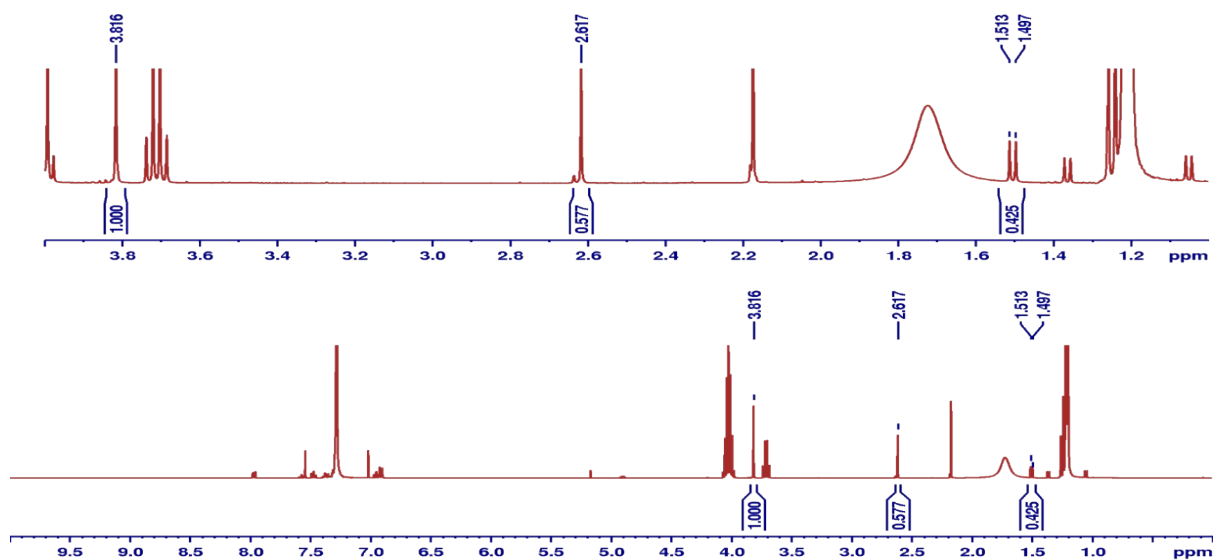


Figure S40. ¹H NMR spectrum (400 MHz, *d*-CDCl₃) of transfer hydrogenation of acetophenone reaction (without a catalyst). Aliquot taken and analysed after at 36 h of reaction. The integral values of the methyl protons of 1-acetylnaphthone and product correspond to the yield of 42% (Table 2, entry 2).

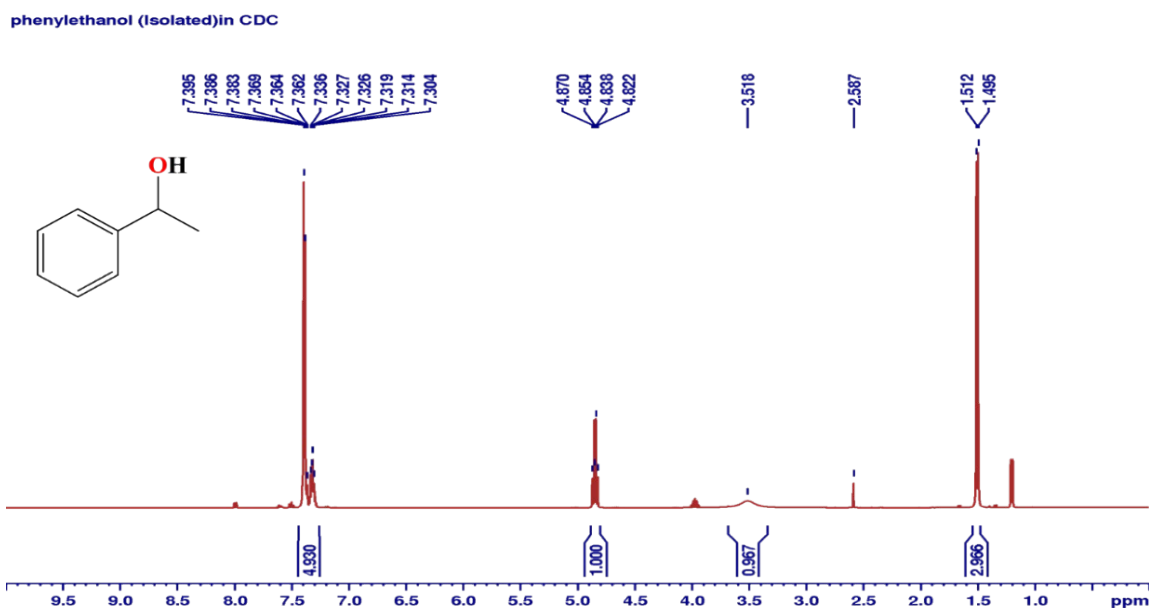


Figure S41. ^1H NMR spectrum of isolated product (1-phenylethanol) from TH of acetophenone. Yield = 0.11 (79%) ^1H NMR spectrum($d\text{-CDCl}_3$): δ (ppm) 1.49 (d, $^3J_{\text{H-H}} = 6.8$ Hz, 3H(CH_3)), 4.89 (q, $^3J_{\text{H-H}} = 6.4$ Hz, 1H(CH)), 4.85 (s, 1H(OH)), 7.30-7.39 (m, cluster 5H_{arom}).

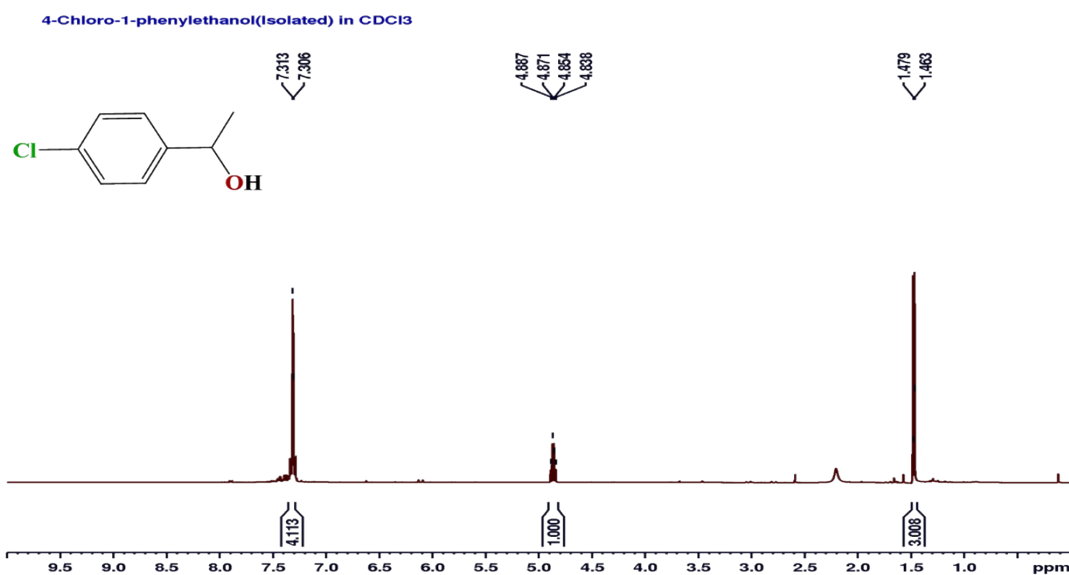


Figure S42. ^1H NMR spectrum of isolated product 1-(4-chloroPhenylethanol) of TH of 4-chloroacetophenone. Yield 0.15 g (97%) = ^1H NMR spectrum($d\text{-CDCl}_3$): δ (ppm) 1.49 (d, $^3J_{\text{H-H}} = 6.8$ Hz, 3H(CH_3)), 4.87 (q, $^3J_{\text{H-H}} = 6.8$ Hz, 1H(CH)), and 7.32 (m, cluster 4H_{arom}).

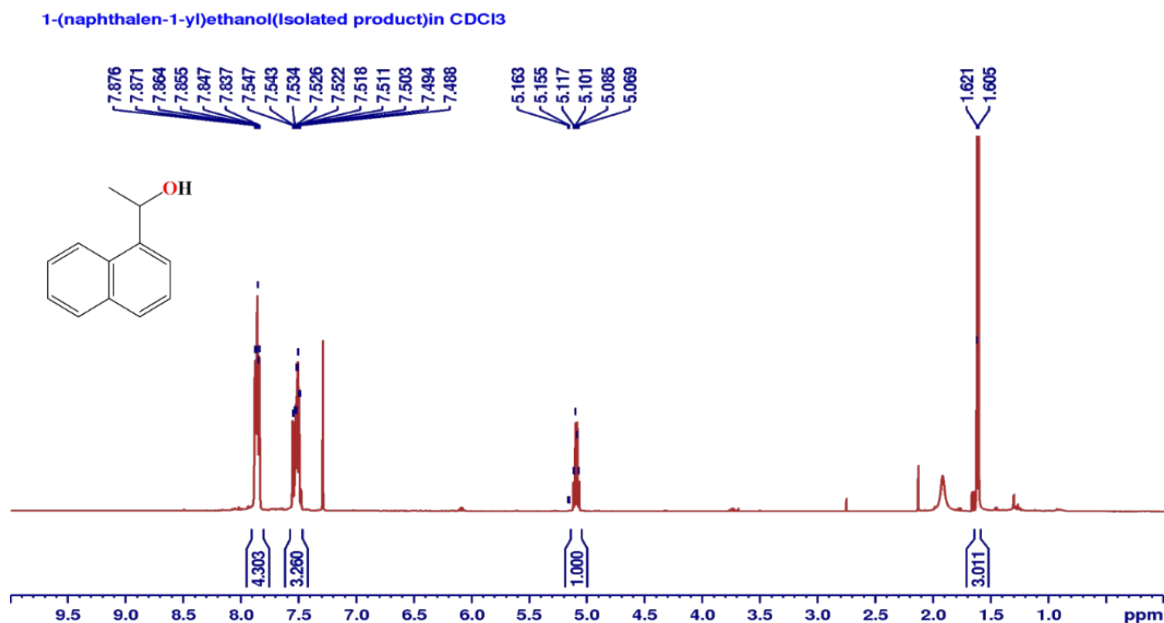


Figure S43. ¹H NMR spectrum of isolated product (1-naphthalen-1-yl)ethanol) from TH of 1-acetylnaphthalenone. 1-(naphthalen-1-yl)ethan-1-ol. Yield 0.14 g (86%) = ¹H NMR spectrum(*d*-CDCl₃): δ(ppm) 1.63 (d, ³J_{H-H} = 6.4 Hz, 3H(CH₃)), 4.98 (q, ³J_{H-H} = 6.4 Hz, 1H(CH)), 7.49-7.55 (m, cluster 2H_{arom}), 7.84-7.88(m, cluster, 4H_{arom}).

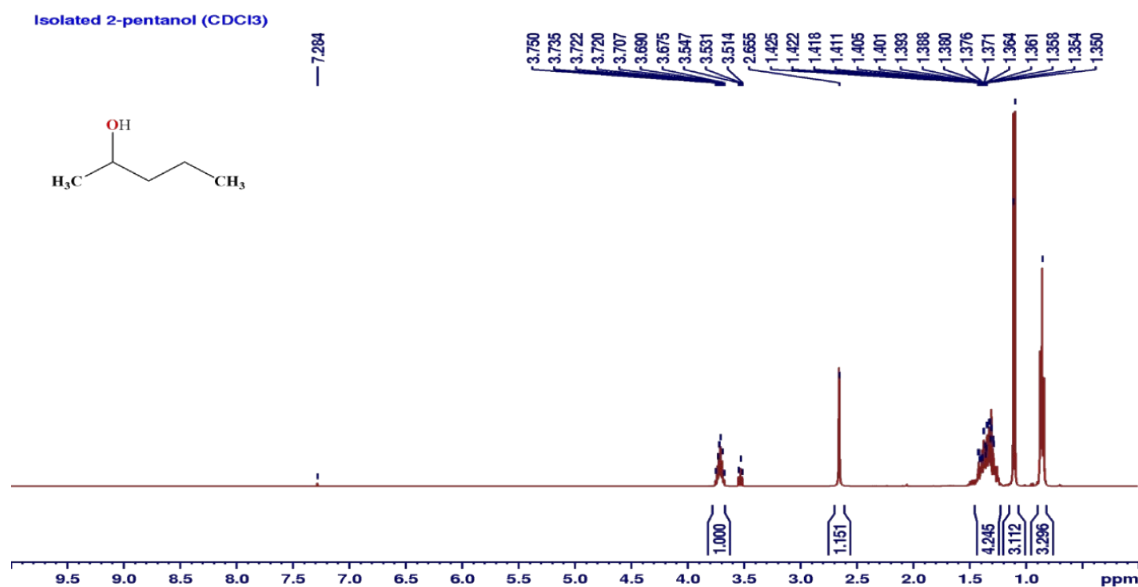


Figure S44. ¹H NMR spectrum of isolated product (2-propanol) from TH of 2-propanone. **2-propanol**. Yield = 0.06 g (67%). ¹H NMR spectrum(*d*-CDCl₃): δ(ppm) 0.89 (d, ³J_{H-H} = 1.6 Hz, 3H(**CH**)), 1.23(t, ³J_{H-H} = 1.6 Hz, 3H(**CH**)), 1.31 (m, ³J_{H-H} = 1.6 Hz, 2H(**CH**)), 1.40(d, ³J_{H-H} = 1.6 Hz, 2H(**CH**)), 4.03 (m, ³J_{H-H} = 1.6 Hz, 1H(**CH**)), 4.89(s, 1H(**OH**)).

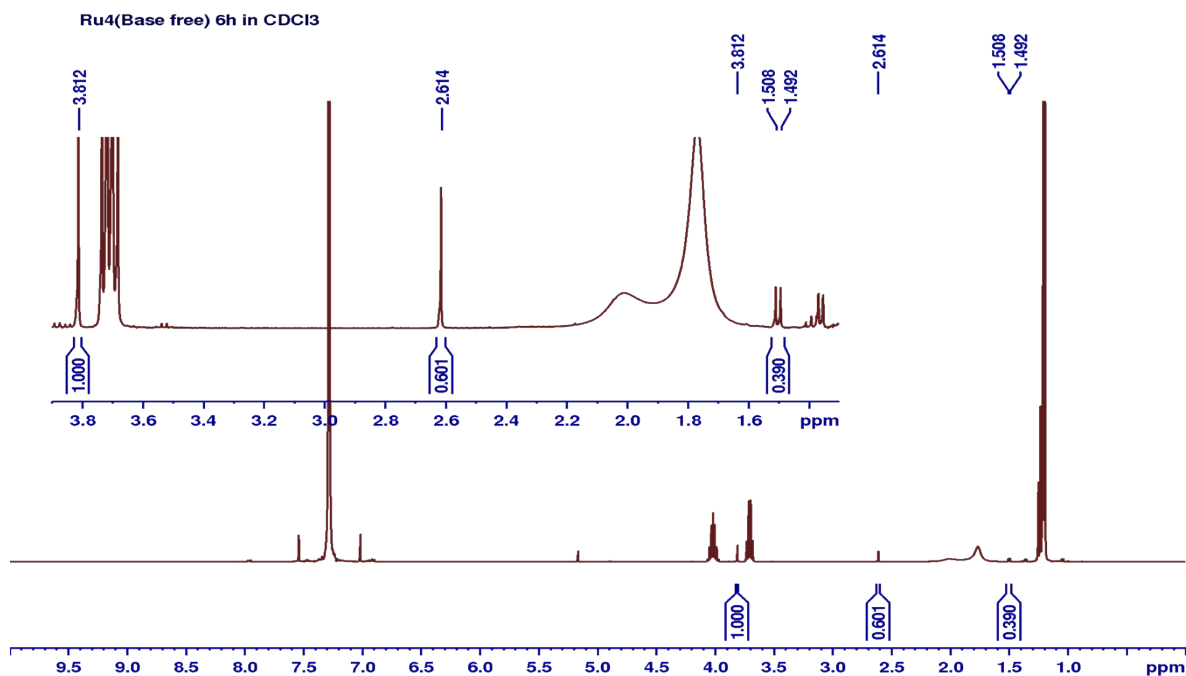


Figure S45. Base free TH of acetophenone catalysed by **Ru4** reaction, time, 6 h corresponding to percentage conversion of 39% (Table 2, entry 3^f).

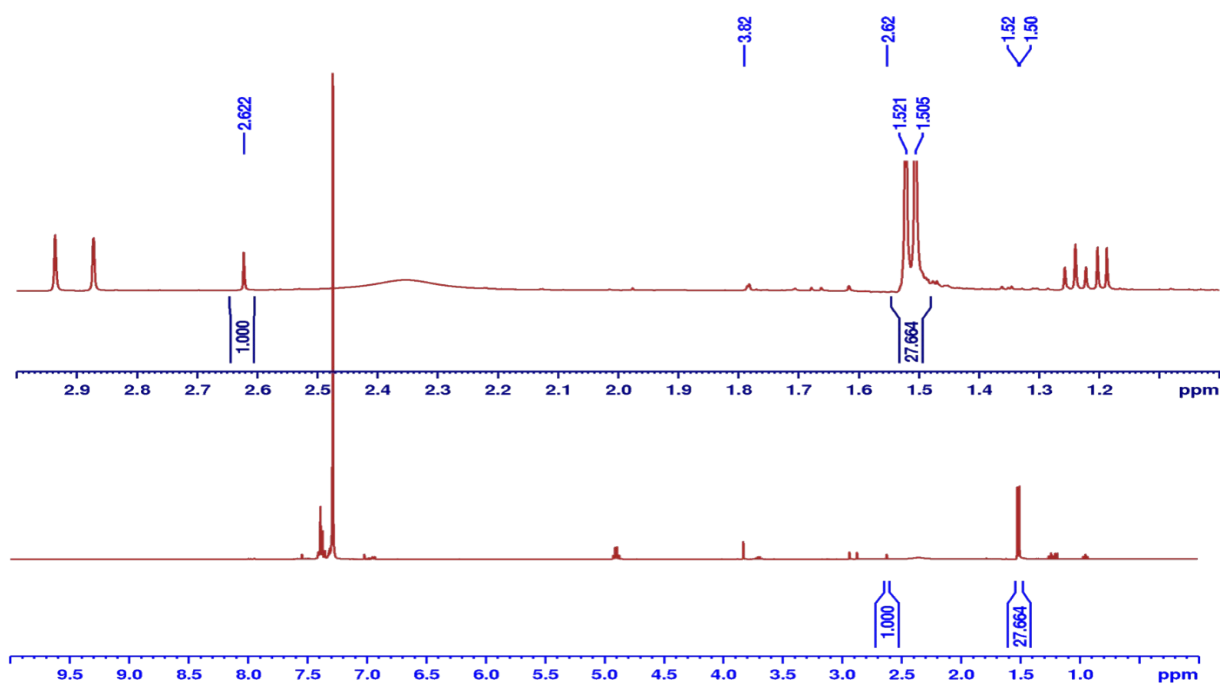


Figure S46. ¹H NMR spectrum (400 MHz, *d*-CDCl₃) of transfer hydrogenation of acetophenone reaction catalysed by **Ru3** with base loading of 100 mol%. Aliquot taken and analysed after at 18 h of reaction. The integral values of the methyl protons of 1-acetylnaphthone and product correspond to the percentage conversion of 97% (Table 2, entry 10).

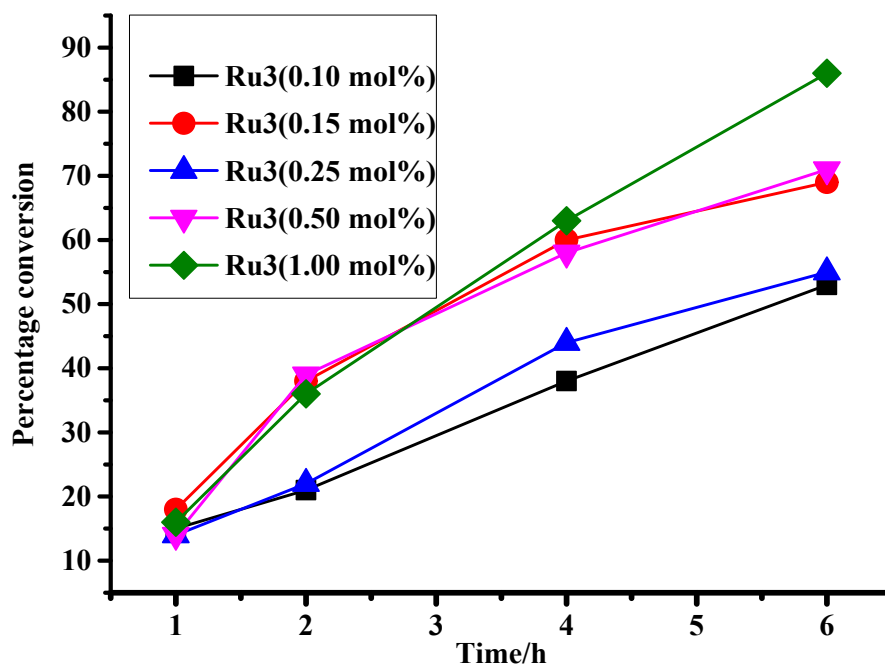


Figure S47. Plots of percentage of conversion vs time showing the effects of catalyst loading on the catalytic activity on transfer hydrogenation of acetophenone reaction using of **Ru₃** as a catalyst.

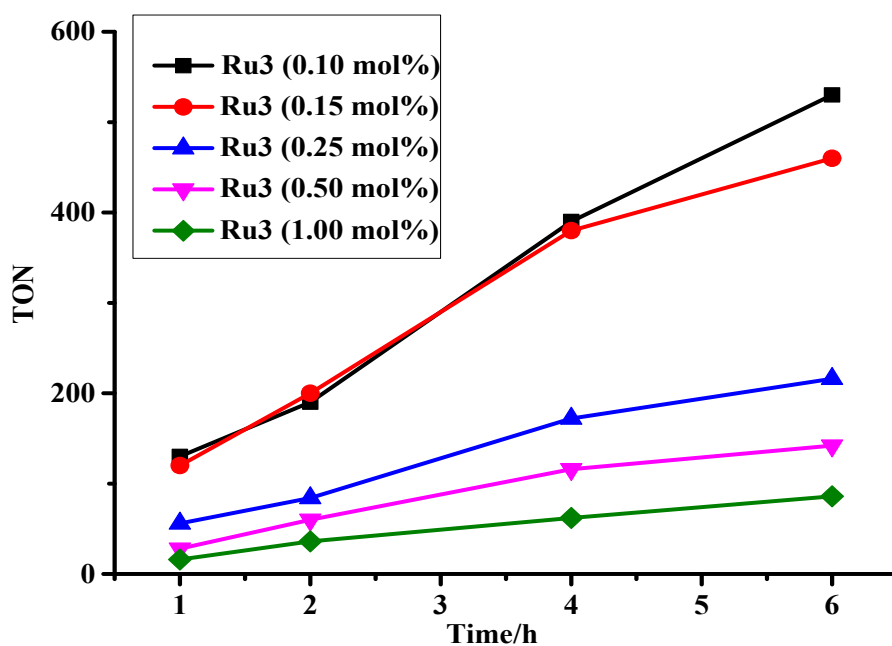


Figure S48. Plots of turnover number (TON) vs time showing the effects of catalyst loading on the catalytic activity of TH of acetophenone reaction using of **Ru3** as a catalyst. Reaction conditions: acetophenone, 1.00 mmol; K^tBuO, 0.100 mmol; ⁱPrOH, 5ml; 82°C, time, 6 h. Percentage Conversion and yield determined by NMR spectroscopy (average of two independent runs), methoxybenzene was used as internal standard.

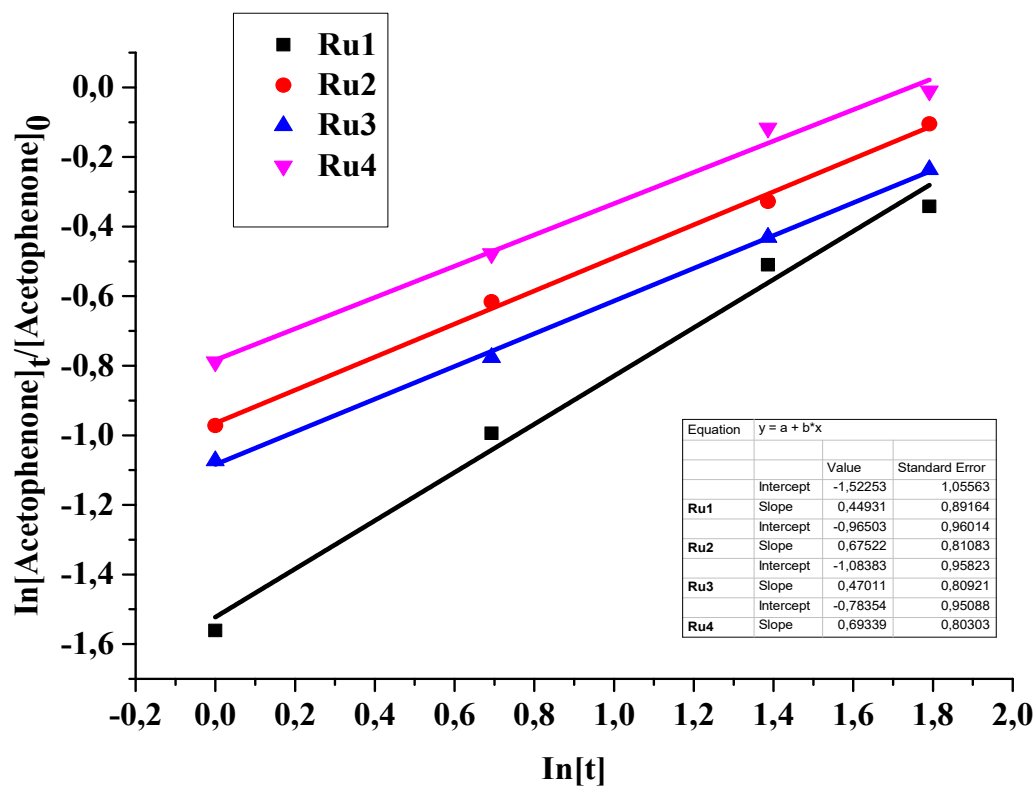


Figure S49. The (a) plot of $\ln[\text{acetophenone}]_t/[\text{acetophenone}]_0$ vs $\ln[t]$ for determination of the rate constants of each catalyst in TH of acetophenone reaction. Condition: acetophenone, 1.00 mmol; *i*PrOH, 5ml; 82°C, time, 6 h. Percentage conversions were determined by NMR spectroscopy (average of two independent runs), methoxybenzene was used as internal standard.